

In Vivo Human Single-Chain Fragment Variable Phage Display-Assisted Identification of Galectin-3 as a New Biomarker of Atherosclerosis

Audrey Hemadou, Alexandre Fontayne, Jeanny Laroche-traineau, Florence Ottones, Philippe Mondon, Stéphane Claverol, Éric Ducasse, Stéphane Sanchez, Sarah Mohamad, Cyril Lorenzato, et al.

▶ **To cite this version:**

Audrey Hemadou, Alexandre Fontayne, Jeanny Laroche-traineau, Florence Ottones, Philippe Mondon, et al.. In Vivo Human Single-Chain Fragment Variable Phage Display-Assisted Identification of Galectin-3 as a New Biomarker of Atherosclerosis. Journal of the American Heart Association, 2021, 10 (19), 10.1161/JAHA.120.016287 . hal-03366155

HAL Id: hal-03366155
https://cnrs.hal.science/hal-03366155

Submitted on 5 Oct 2021

HAL is a multi-disciplinary open access archive for the deposit and dissemination of scientific research documents, whether they are published or not. The documents may come from teaching and research institutions in France or abroad, or from public or private research centers.

L'archive ouverte pluridisciplinaire **HAL**, est destinée au dépôt et à la diffusion de documents scientifiques de niveau recherche, publiés ou non, émanant des établissements d'enseignement et de recherche français ou étrangers, des laboratoires publics ou privés.



Distributed under a Creative Commons Attribution - NonCommercial 4.0 International License

Journal of the American Heart Association

ORIGINAL RESEARCH

In Vivo Human Single-Chain Fragment Variable Phage Display-Assisted Identification of Galectin-3 as a New Biomarker of Atherosclerosis

Audrey Hemadou, PhD; Alexandre Fontayne, PhD; Jeanny Laroche-Traineau, PhD; Florence Ottones, PhD; Philippe Mondon, PhD; Stéphane Claverol, PhD; Éric Ducasse, MD, PhD; Stéphane Sanchez, HSD; Sarah Mohamad, MSc; Cyril Lorenzato, PhD; Martine Duonor-Cerutti, PhD; Gisèle Clofent-Sanchez, PhD*; Marie-Josée Jacobin-Valat, PhD*

BACKGROUND: Atherosclerosis is a complex pathology in which dysfunctional endothelium, activated leucocytes, macrophages, and lipid-laden foam cells are implicated, and in which plaque disruption is driven by many putative actors. This study aimed to identify accurate targetable biomarkers using new in vivo approaches to propose tools for improved diagnosis and treatment.

METHODS AND RESULTS: Human scFv (single-chain fragment variable) selected by in vivo phage display in a rabbit model of atherosclerosis was reformatted as scFv fused to the scFv-Fc (single-chain fragment variable fused to the crystallizable fragment of immunoglobulin G format) antibodies. Their reactivity was tested using flow cytometry and immunoassays, and aorta sections from animal models and human carotid and coronary artery specimens. A pool of atherosclerotic proteins from human endarterectomies was co-immunoprecipitated with the selected scFv-Fc followed by mass spectrometry for target identification. Near-infrared fluorescence imaging was performed in *Apoe*$^{-/-}$ mice after injection of an Alexa Fluor 647–labeled scFv-Fc-2c antibody produced in a baculovirus system with 2 additional cysteine residues (ie, 2c) for future coupling to nano-objects for theranostic applications. One scFv-Fc clone (P3) displayed the highest cross-reactivity against atherosclerotic lesion sections (rabbit, mouse, and human) and was chosen for translational development. Mass spectrometry identified galectin-3, a β-galactoside-binding lectin, as the leader target. ELISA and immunofluorescence assays with a commercial anti-galectin-3 antibody confirmed this specificity. P3 scFv-Fc-2c specifically targeted atherosclerotic plaques in the *Apoe*$^{-/-}$ mouse model.

CONCLUSIONS: These results provide evidence that the P3 antibody holds great promise for molecular imaging of atherosclerosis and other inflammatory pathologies involving macrophages. Recently, galectin-3 was proposed as a high-value biomarker for the assessment of coronary and carotid atherosclerosis.

Key Words: biomarkers ■ flow cytometry ■ human antibodies ■ imaging ■ in vivo phage display

Downloaded from http://ahajournals.org by on October 1, 2021

Atherosclerosis, the main cause of death in Western countries, is a chronic and inflammatory disease characterized by the buildup of lipid-rich plaques that clog the arteries. Atherosclerotic lesions result from the local accumulation of lipids, immune and nonimmune cells, and cellular debris.[1] Endothelial cells, activated by lipoproteins, express chemokines and adhesion molecules that contribute to the recruitment of

Correspondence to: Marie-Josée Jacobin-Valat and Audrey Hemadou, Centre de Resonance Magnétique des Systèmes Biologiques (CRMSB) 146 rue Léo Saignat, Batiment 4A, 33076 Bordeaux, France. E-mails: marie-josee.jacobin-valat@rmsb.u-bordeaux.fr; audrey.hemadou@orange.fr

Supplementary Material for this article is available at https://www.ahajournals.org/doi/suppl/10.1161/JAHA.120.016287

†G. Clofent-Sanchez and M.-J. Jacobin-Valat contributed equally.

For Sources of Funding and Disclosures, see page 17.

© 2021 The Authors and LFB Biotechnologies. Published on behalf of the American Heart Association, Inc., by Wiley. This is an open access article under the terms of the Creative Commons Attribution-NonCommercial License, which permits use, distribution and reproduction in any medium, provided the original work is properly cited and is not used for commercial purposes.

JAHA is available at: www.ahajournals.org/journal/jaha

CLINICAL PERSPECTIVE

What Is New?

- This study highlights the potential of in vivo phage display for the discovery of new targetable biomarkers of atheroma plaque progression in the pathological microenvironment. Our findings show that galectin-3 is an ideal molecular biomarker that can be targeted for diagnostic purposes.
- P3 is the first human recombinant antibody that recognizes galectin-3 both in animal models of atherosclerosis and in human specimens of atherosclerotic arteries and that can be easily used for translational development.
- Manipulating the genes of the variable regions allowed the development of a format suitable for in vivo studies after coupling to theranostic nano-objects.

What Are the Clinical Implications?

- It is crucial to identify vulnerable patients at a higher risk of developing coronary and carotid atherosclerosis.
- The human antibody against galectin-3, which plays a key role in atherosclerosis pathogenesis, discovered in this study by combining in vivo phage display and proteomics could be a useful tool for developing a novel molecular imaging modality.
- However, more studies are needed to better understand galectin-3's role (beneficial or detrimental) in atheroma plaque formation to determine its therapeutic potential, in addition to its confirmed potential as diagnostic biomarker for atherosclerosis or for inflammatory pathologies that involve macrophages.

Nonstandard Abbreviations and Acronyms

LOX1	lectin-type oxidized low-density lipoprotein receptor 1
scFv	single-chain fragment variable
scFv-Fc	single-chain fragment variable fused to the crystallizable fragment of immunoglobulin G format

monocytes. Monocytes then differentiate into macrophages that express scavenger receptors and CD36 molecules and uptake oxidized low-density lipoprotein (LDL), leading to the formation of foam cells, the precursors of plaque instability and vulnerability.[2,3]

To improve atherosclerosis diagnosis and treatment, the identification of new targetable biomarkers is crucial. Currently, the diagnosis of atheroma plaques is invasive and is often done only at advanced disease stages. Recently, we developed contrast agents functionalized with antibody fragments to target platelets and loaded with iron oxide for noninvasive magnetic resonance molecular imaging. These targeting objects can specifically recognize the atheroma plaque in *Apoe*$^{-/-}$ mice ex vivo and in vivo.[4]

To identify new targetable proteins that are overexpressed in the atheroma plaque, we recently set up an in vivo phage display method to select antibody fragments from a human scFv (single-chain fragment variable) library (MG-Umab[5]) in an hypercholesterolemic rabbit model.[6] The in vivo discovery of biomarkers by this approach should allow better understanding atherosclerosis pathogenesis and development of new tools for imaging modalities. Moreover, human antibodies show limited immunogenicity when used in the clinic. After high-throughput flow cytometry analysis, this method led to the selection and retrieval of 142 scFv-phages with complete and in-frame VH and VL germline genes (Sanger sequencing of the whole scFv fragment). Immunohistochemistry experiments confirmed the ex vivo reactivity of 60% of these scFv-phages in sections of rabbit aorta with atheroma.[6]

Here, we characterized some of these selected in vivo human antibodies produced in HEK293 cells (scFv-Fc [scFv fused to the crystallizable fragment of immunoglobulin G format]) to confirm their reactivity by flow cytometry assays with rabbit atheroma protein extracts and by immunohistochemistry using rabbit and mouse aorta sections and human endarterectomy specimens. Importantly, we selected only the antibodies that recognized atheroma in arterial tissue sections from 2 preclinical models and in human endarterectomy biopsies.

We then focused on P3 scFv-Fc because of its high cross-reactivity against protein extracts from atherosclerotic lesions in all tested species, and because it was highly represented during the in vivo phage-display selection, as reported in our previous work using third-generation next-generation sequencing.[7] By mass spectrometry and ELISA assays, we identified galectin-3 as the P3 scFv-Fc target. Galectin-3, a member of β-galactoside-binding proteins, plays key roles in several physiological and pathophysiological processes.[8] Besides its expression in endothelial cells, galectin-3 is also overexpressed by macrophages, the main inflammatory cells in the atheromatous plaque,[9,10] and is involved in monocyte attraction and macrophage activation.[11] In agreement, we found that P3 scFv-Fc and an antibody against the macrophage receptor LOX1 (lectin-type oxidized LDL receptor 1) colocalized in human endarterectomy sections.

Finally, we showed the ex vivo binding of P3 scFv-Fc to its target in atherosclerotic aorta of *Apoe*$^{-/-}$ mice by

Downloaded from http://ahajournals.org by on October 1, 2021

fluorescence. Because it has been suggested that the expression of galectin-3 fluctuates during plaque progression,[9] our findings could lead to the development of novel specific contrast agents functionalized with the P3 human antibody for noninvasive preclinical imaging of atherosclerosis and other inflammatory diseases.

METHODS

The data and analytical methods will be made available to other researchers for purposes of reproducing the results or replicating the procedure. However, because of a patent, study materials will not be made available to other researchers.

Animal Models

All animal experiments were performed in accordance with the *Guide for the Care and Use of Laboratory Animals* (NIH publication no. 85-23, revised 1996) and were approved by the Bordeaux Ethics Committee (CEEA50). All preclinical experiments described in this publication were approved by the Animal Care and Use Committee of Bordeaux, France (no. 50120192-A).

Adult male New Zealand White rabbits, weighing between 2.5 and 3.0 kg, were obtained from Charles Rivers Laboratories (St. Germain sur l'Arbresle, France). For 6 to 8 months, rabbits were fed a fat atherogenic diet that included 0.3% (w/w) cholesterol. To promote the development of complicated plaques, rabbits were subject to a surgical inflammatory injury 1 to 2 months after the beginning of the diet. De-endothelialization of thoracic and abdominal aortic areas was mechanically induced by 3 inflations and retractions of a 4-F Fogarty balloon catheter (Edwards Lifesciences, Maurepas, France). Surgery was performed under anesthesia induced by intramuscular injection of 50 mg/kg ketamine (Merial, France) and 5 mg/kg xylazine (Bayer Healthcare, France) and maintained by mask inhalation of 1.5% to 2% of isoflurane. Preventive antithrombotic treatment was heparin sodium solution (1000 IU) (Heparin Choay; Sanofi Synthelabo, Paris, France). Preoperative and postoperative analgesia were performed by administration of 100 mg of aspirin (Injectable Aspegic; Sanofi Synthelabo), and tolfedine (4 mg/kg; 2 subcutaneous injections 48 hours apart), respectively.[12] Rabbits were euthanized by a single intravenous injection of pentobarbital in the marginal ear vein (120 mg/kg) (CEVA Santé Animale, France).

Female, 6-week-old *Apoe*$^{-/-}$ mice (17–18 g in weight) were purchased from Charles River Laboratories (Saint Germain Nuelles, France) and housed under a 12-hour light/dark cycle with food and water provided ad libitum. Mice were fed a high cholesterol diet (0.15% cholesterol) for 24 weeks to promote the development of atherosclerotic lesions. Animals were cared for in accordance with the institutional guidelines, and they were familiarized with their environment for at least 7 days before initiation of any experiments. For ex vivo studies and aorta isolation, animals were euthanized by intraperitoneal injection of Exagon (Axience, France) (300 mg/kg), diluted with 0.9% NaCl (1:4) under general anesthesia with 5% isoflurane.

Human Specimen Collection

Human tissue specimens were provided by Dr Ducasse, vascular surgeon at CHU Pellegrin Hospital (Bordeaux, France). Human samples were from patients who underwent endarterectomy after an acute vascular event. Human coronary artery samples were harvested from patients with end-stage heart failure during heart transplantation. All clinical interventions took place at CHU Pellegrin (Bordeaux, France) and at Haut-Lévèque Hospital (Pessac, France). All work with human tissues was approved by the Bordeaux Ethics Committee (Committee for the Protection of Persons Southwest and Overseas) and by the Research Ministry in France (authorization no. DC –2016-2724). The Bordeaux ethics committee waived the need for the patient written consent because surgical waste no longer attached to the person is considered res nullius. Patients were informed by the clinicians; if they did not express their opposition to research, the deidentified samples were immediately processed (paraffin embedding or protein extraction). All study procedures complied with the ethical standards of the Declaration of Helsinki.

In Vivo Selection of scFv-Phages and Screening by Flow Cytometry of Individual Clones

In Vivo Selection

ScFv-phages from the optimized (in-frame scFv selection) MG-Umab library (fully human scFv)[5,13] were selected by in vivo phage display in the rabbit model of atherosclerosis. The scFv-phages were isolated from atherosclerotic lesions, located from the aortic arch to the iliac bifurcations. Briefly, they were recovered from the endothelial layer and then from the intratissular (ie, subendothelial layer in the intima) and intracellular (ie, cells in the plaque, such as macrophages, foam cells, T cells) fractions after extensive washes between each fraction. This process was repeated for each round of biopanning. Three cycles of selection were performed to enrich for specific antibodies, as described in our previous studies.[6,7] Then, the in vivo–selected scFv-phages were screened by flow cytometry for the identification of clones of interest.[6]

Downloaded from http://ahajournals.org by on October 1, 2021

Flow Cytometry Screening

Rabbit Protein Extraction and Coupling to Magnetic Beads

Protein extraction from rabbit atherosclerotic lesions was performed as previously described.[12] Briefly, proteins were solubilized with the T-PER lysis buffer (Thermo Fisher Scientific, France) complemented with a protease inhibitor cocktail (Thermo Fischer Scientific) and a Polytron TP-20 Homogenizer 8 (Kinematica, Lucerne, Switzerland). After 2 centrifugation steps at 13 000*g* at 4°C for 45 minutes to discard the insoluble material in the supernatant, the protein concentration of every soluble extract was determined using the Bradford Assay Kit, according to the manufacturer's instructions (Thermo Fisher Scientific).

Fifty micrograms of protein extracts were covalently coupled to 300 nm of magnetic Carboxyl Adembeads according to the manufacturer's instructions (Ademtech, France). Three batches of protein-coupled beads per sample were used.

Phage Antibody Preparation

Individual phage-infected XL1 blue bacteria were grown in 96-well plates (Greiner Bio One, France) in 500 µL triptone/yeast extract (2TY)/ampicillin/5% glucose supplemented with 10 µg/mL tetracycline. After overnight incubation, 25 µL of bacterial culture were inoculated in 500 µL 2xTYGAT medium and incubated for 3 hours. Phage production was induced by adding 25 µL of 2TY containing 3.10^8 M13KO7 helper phage particles (Stratagene, France). After infection at 37°C for 1 hour, bacteria were pelleted, resuspended in 500 µL 2TY/ampicillin/5% glucose medium supplemented with 40 µg/mL kanamycin, and grown at 26°C under rotation (New Brunswick Scientific, Edison, NJ) overnight. Bacteria were spun down at 10 000*g* for 10 minutes, and supernatants were used immediately for flow cytometry assay.

scFv-Phage Screening by Flow Cytometry

Binding of scFv-phages or scFv-Fc fusion antibodies to atherosclerotic protein extracts was determined by flow cytometry. Forty microliters of atherosclerotic rabbit protein-coated beads (5 µg/mL) were added to 100 µL of scFv-phages and incubated at 4°C under rotation for 3 hours. This was followed by incubation with mouse anti-pVIII (Abcam, France) or rabbit anti-human Fcγ (Jackson Immunoresearch, USA) primary antibodies (1:1000) at 4°C under rotation overnight, and by incubation with Alexa Fluor 488– labeled anti-mouse antibodies (Life Technologies, France) (1:40) for scFv-phage detection.

Validation of the scFv Fragment VH-VL Sequences by Sequencing

Sanger sequencing was performed using primers for the scFv flanking regions in the phagemid (5′-TGCAAATTCTATTTCAAGGAGAC-3′ and 5′-AGA ATCATCAGATAAAGTAATCC-3′). Antibody gene fragments were analyzed using the IMGT/V-QUEST database (www.imgt.org/IMGT_vquest/vquest) for V germline determination and Complementarity-Determining Region analyses.[14]

Production of Recombinant scFv-Fc Antibodies in HEK-293 FreeStyle and Baculovirus Expression Systems

Antibody Production and Purification From HEK-293 Cells

ScFv-Fc was produced by transient transfection using the FreeStyle 293-F expression system (Invitrogen, France). Expression vectors were prepared by producing (using Invitrogen GeneArt) the scFv-encoding cDNA fragments as linear fragments with optimized codons for *Homo sapiens*. HEK-293 FreeStyle cells were transfected with the purified expression vectors, according to the supplier instructions, with PEI 250 kDa (Sigma-Aldrich) at 1:2 ratio (DNA:transfection reagent). After 7 days of production at 37°C and 8% CO_2 in F17 medium supplemented with 8 mmol/L glutamine, scFv-Fc antibodies were purified by 1-step affinity chromatography with HiTrap FF protein A (GE Healthcare, France) on an ÄKTA avant 80 chromatography system. Molecules were eluted with 25 mmol/L citrate, pH3.0, and dialyzed against PBS, filtered (0.2 µm), and stored at 4°C until use.

Antibody Production and Purification From Insect Cells

The fusion ScFv-Fc P3 with 2 cysteine residues (scFv-Fc-2c) was produced using the baculovirus expression system.[15] Briefly, the cDNA encoding the P3 scFv was polymerase chain reaction–amplified with the following forward and reverse primers: 5′-GCTACTTAAGG GTGTCCAGTGCCAGGTGCAGCTGCAGCAGTCTGG ACCCGG-3′ and 5′-GCTACGTACGCTTGATTTCCA GCTTGGTGCCGCCT- 3′. The polymerase chain reaction fragment was inserted into a specific transfer vector in frame with the sequence encoding the immunoglobulin (Ig) G1 signal peptide at the 5′ end and with a cDNA encoding the human IgG1 fragment variable domain with 2 extra cysteine residues at the C-terminus. Sf9 cells were cotransfected by lipofection with the transfer vector and purified viral DNA in the presence of 40 µL of DOTAP liposomal transfection reagent (Roche). Recombinant viruses were isolated by plaque assay. ScFv-Fc-2c was produced by infecting Sf9 cells, adapted to grow in serum-free medium, with the selected recombinant virus at a multiplicity of infection of 3 plaque-forming units per cell. At day 3 after infection, cell culture supernatant was harvested, and scFv-Fc-2c was purified using HiTrap FF, protein A, as

Downloaded from http://ahajournals.org by on October 1, 2021

recommended by the manufacturer (GE Healthcare), and an ÄKTA purifier system. ScFv-Fc-2c was filter-sterilized through a 0.22 µm filter (Millex GP; Millipore) and stored at 4°C until use.

Reactivity Analysis of scFv-Fc Clones by Flow Cytometry and Immunohistochemistry

Flow Cytometry Analyses

Maintenance of reactivity after scFv-Fc reformatting was first assessed by flow cytometry using the same protocol described for scFv-phages. Briefly, scFv-Fc was diluted at 10 µg/mL in PBS buffer and incubated with beads coated with protein extracts from rabbit atherosclerotic lesions (5 µg/mL) at 4°C under rotation for 3 hours. This was followed by incubation with rabbit anti-human Fcγ primary (1:65 dilution; Jackson Immunoresearch) and Alexa Fluor 488–labeled anti-rabbit (1:30 dilution, Life Technologies) secondary antibodies.

Immunohistochemistry Analysis of Rabbit and Mouse Aorta Tissue Sections and of Human Endarterectomy Specimens

The immunoreactivity of scFv-Fc antibodies was evaluated using tissue sections prepared from paraffin-embedded human, mouse, and rabbit atheromatous plaque specimens. Tissue sections were deparaffinized and rehydrated. Blocking steps (H_2O_2 blocking and unspecific site blocking with PBS/1% BSA/0.2% Triton X-100) and a retrieval step (10 mmol/L Tris, 1 mmol/L EDTA, 0.05% Tween 20, pH9) were performed. For human tissue sections, another blocking step was performed by incubation with 5% goat serum and the $F(ab')_2$ fragment goat anti-human IgG (Heavy +Light chains) (Jackson Immunoresearch) and goat anti-human IgG (Fcγ specific) (Jackson Immunoresearch), diluted at 100 µg/mL. After washes with PBS/1% BSA, sections were incubated with the scFv-Fc antibodies at 10 µg/mL at 4°C overnight. After washes with PBS/1% BSA/0.025% Triton X-100, sections were incubated with the secondary horseradish peroxidase–conjugated goat anti-human (Fcγ specific) antibody (1:1000) (Jackson Immunoresearch). Negative control samples were incubated with only the secondary antibody. Antibody binding was revealed using the 3,3'-diaminobenzidine system (DAKO, France).

Target Identification by Immunoprecipitation and Mass Spectrometry Analysis

Coimmunoprecipitations

The Invitrogen Dynabeads co-immunoprecipitation kit (14321D; Thermo Fisher Scientific) was used following the manufacturer's instructions. Briefly, 20 µg of P3 scFv-Fc or C4 scFv-Fc (control antibody) or 10 µg of a commercial Gal3 Ab antibody (anti-galectin-3) (Abcam) was added to 1 mg of Dynabeads in coupling buffer and incubated at 37°C under rotation overnight. Proteins from human endarterectomy specimens were extracted and solubilized following the same protocol used for proteins from rabbit atherosclerotic lesions. After extraction, proteins were pooled and stored at −80°C. Dynabeads/antibody (P3 or C4) complexes were equilibrated in extraction buffer and then incubated with 1 mg of pooled human protein homogenates at 4°C under rotation for 1 hour. The Dynabeads/commercial Gal3 Ab complexes were incubated with 3 µg of Gal3R (recombinant human galectin-3). Then, beads were washed, and the co-immunoprecipitated proteins were eluted in the elution buffer (2xSDS Laemmli buffer supplied with the kit). One aliquot of each eluate was directly analyzed by SDS-PAGE polyacrylamide gel (4%–10%) and stained with silver nitrate. The rest of each sample was sent to a mass spectrometry facility for further processing.

Mass Spectrometry Analysis

Sample Preparation and Protein Digestion

Samples were solubilized in Laemmli buffer and were concentrated and cleaned on SDS-PAGE gels. Separation was stopped when proteins entered the resolving gel. After colloidal blue staining, all of the bands present in the relevant lane were extracted from the SDS-PAGE gel and cut in 1×1-mm pieces. Gel pieces were destained in 25 mmol/L ammonium bicarbonate 50% acetonitrile (ACN), rinsed twice in ultrapure water, and shrunk in ACN for 10 minutes. After ACN removal, gel pieces were dried at room temperature, covered with trypsin solution (10 ng/µL in 50 mmol/L NH_4HCO_3), rehydrated at 4°C for 10 minutes, and incubated at 37°C overnight. They were then incubated in 50 mmol/L NH_4HCO_3 at room temperature with rotary shaking for 15 minutes. Supernatants were collected, and the H_2O/ACN/HCOOH (47.5:47.5:5) extraction solution was added to the gel slices for 15 minutes. The extraction step was repeated twice. Supernatants were pooled and dried in a vacuum centrifuge. Digests were solubilized in 0.1% HCOOH.[16,17]

Nano-Scale Liquid Chromatographic Tandem Mass Spectrometry Analysis and Label-Free Quantitative Data Analysis

Peptide mixtures were analyzed with an UltiMate 3000 nano–liquid chromatography system (Dionex, Amsterdam, the Netherlands) coupled to an Electrospray Orbitrap Fusion Lumos Tribrid Mass Spectrometer (Thermo Fisher Scientific). Ten microliters of peptide digests were loaded onto a 300-µm-ID×5-mm C_{18}

Downloaded from http://ahajournals.org by on October 1, 2021

PepMap trap column (LC Packings) at a flow rate of 10 µL/min. Peptides were eluted from the trap column onto an analytical 75-mm-ID×50-cm C18 Pep-Map column (LC Packings) with a 4% to 40% linear gradient of solvent B in 48 minutes (solvent A was 0.1% formic acid and solvent B was 0.1% formic acid in 80% ACN). The separation flow rate was set at 300 nL/min. The mass spectrometer operated in positive ion mode at 1.8-kV needle voltage. Data were acquired using the Xcalibur 4.1 software in data-dependent mode. Mass spectrometry (MS) scans (m/z 375–1500) were recorded at a resolution of R=120 000 (at m/z 200) and an automatic gain control target of 4×10^5 ions collected within 50 milliseconds. Dynamic exclusion was set to 60 seconds, and top speed fragmentation in higher-energy C-trap dissociation (HCD) mode was performed over a 3-second cycle. Tandem Mass Spectrometry (MS/MS) scans with a target value of 3×10^3 ions were collected in the ion trap with a maximum fill time of 300 milliseconds. Additionally, only +2 to +7 charged ions were selected for fragmentation. Other settings were as follows: no sheath, no auxiliary gas flow, heated capillary temperature=275°C, normalized HCD collision energy=30%, and isolation width=1.6 m/z. The monoisotopic precursor selection was set to peptide and the intensity threshold to 5×10^3.

Database Search and Result Processing

The obtained data were analyzed with SEQUEST and Proteome Discoverer 2.3 (Thermo Fisher Scientific) using the *Homo sapiens* Reference Proteome Set (from Uniprot 2019-05; 73 645 entries). Spectra from peptides higher than 5000 Da or lower than 350 Da were rejected. The search parameters were as follows: mass accuracy of the monoisotopic peptide precursor and of peptide fragments was set to 10 ppm and 0.6 Da, respectively. Only b- and y-ions were considered for mass calculation. Methionine oxidation (+16 Da) and N-terminal acetylation (+42 Da) were considered as variable modifications and cysteine carbamidomethylation (+57 Da) as fixed modification. Two missed trypsin cleavages were allowed. Peptide validation was performed with the Percolator algorithm,[18] and only high-confidence peptides were retained (ie, false positive rate=1% at the peptide level). Peaks were detected and integrated using the Minora algorithm embedded in Proteome Discoverer.

ELISA Assay

Three independent ELISA assays were performed in triplicate. ELISA plates were coated (at 4°C overnight) with recombinant human galectin-3 (Abcam), galectin-3BP (Abcam), galectin-1 (Abcam), GPαIIbβ3 integrin (Enzyme Research Laboratory, UK), or BSA (all at 5 µg/mL diluted in carbonate buffer). Then, each well was blocked with PBS/5% milk at 37°C for 1 hour. A mouse antibody against galectin-1 (Abcam) and rabbit antibodies against human galectin-3 and galectin-3BP (Abcam) and the mouse AP2 antibody (a gift from Dr Nurden) against the glycoprotein αIIbβ3 (GPαIIbβ3) integrin were used as positive controls. The human P3 scFv-Fc and control negative (CN) scFv-Fc (irrelevant antibody, a gift from Laboratoire Français du Fractionnement et des Biotechnologies antibodies (diluted to 50 µg/mL), and the commercial antibodies (diluted to 10 µg/mL) were added to the respective wells at room temperature for 2 hours, followed by horseradish peroxidase–conjugated secondary antibodies. Each step was followed by extensive washes in PBS/0.1% Tween 20. The final wash was with PSB alone, and the antibody reaction was evaluated with the o-phenylenediamine dihydrochloride system for ELISA (Sigma-Aldrich). Color absorbance was immediately read at 405 nm in a plate reader (Chameleon; Thermo Fisher Scientific).

Co-staining Experiments

Human Tissue Sections

Paraffin-embedded atherosclerotic lesions from human endarterectomy and coronary artery specimens were used in co-staining experiments. All of the steps including the retrieval process and classical blocking steps were as described for immunohistochemistry. The following antibody combinations were used: (1) P3 scFv-Fc diluted to 50 µg/mL in PBS/1% BSA with the anti-human galectin-3 antibody (10 µg/mL) (Abcam), and (2) P3 scFv-Fc diluted to 50 µg/mL in PBS/1% BSA with the rabbit anti-human LOX1 antibody (5 µg/mL). After incubation with these antibody combinations at 4°C overnight, sections were washed and then incubated (room temperature for 1 hour) with the following secondary fluorescent antibodies: Alexa Fluor 568–labeled anti-human (1:200) for P3 scFv-Fc, Alexa Fluor 488–labeled anti-rabbit (1:1000) for the anti-LOX1 antibody, or Alexa Fluor 488–labeled anti-mouse (1:200) for the anti-galectin-3 antibody. After washes, sections were mounted with Vectashield (VWR, France).

For all experiments, adjacent sections incubated only with secondary antibodies were used as a negative control.

Images were acquired with a Nanozoomer 2.0 HT slide scanner and the fluorescence imaging module (Hamamatsu Photonics, France) using an UPS APO 20X NA 0.75 objective and an additional 1.75× lens, leading to a final magnification of 35×. Virtual slides were acquired with a TDI-3CCD camera. Fluorescent images were acquired with a mercury lamp (LX2000 200W; Hamamatsu Photonics, Massy, France), and the filter was set for DAPI and/or GFP (green fluorescent protein)/Alexa Fluor 488, and/or Alexa Fluor 568, and/or Alexa FLuor 647/Cy5 fluorescence.

Downloaded from http://ahajournals.org by on October 1, 2021

Mouse Tissue Sections

For immunofluorescence co-staining of atherosclerotic lesions from *Apoe*$^{-/-}$ mouse aorta samples, the following antibodies were tested (at 4°C overnight): P3 scFv-Fc (diluted to 50 µg/mL in PBS/1% BSA) and rabbit anti-LOX1 antibody (5 µg/mL). After washes and incubation (room temperature for 1 hour) with the secondary fluorescent antibodies Alexa Fluor 647–labeled anti-human (1:100) for scFv-Fc and Alexa Fluor 488 anti-rabbit (1:1000) for the anti-LOX1 antibody, sections were washed, stained with DAPI (Thermo Fisher Scientific), and mounted with ProLong Gold (Life Technologies).

For all experiments, adjacent sections incubated only with secondary antibodies were used as negative controls.

Ex Vivo Fluorescence Imaging of P3 scFv-Fc-2c

The chests of 3 mice (n=2 *Apoe*$^{-/-}$ and n=1 control) were opened by thoracotomy, the heart exposed, and the right atrium cut. A 30-gauge needle was inserted in the left ventricle. PBS/heparin (50 IU/mL per 2.5 mL; Sanofi Aventis, France) was inoculated, followed by 10 mL of PBS. Perfusion was continued with 2 mL of PBS containing the human P3 scFv-Fc-2c or the control human IgG antibody (100 µg for both) coupled to Alexa Fluor 647 according to the manufacturer's instructions and using the Alexa Fluor 647 Antibody Labeling Kit (Thermo Fisher Scientific). After 20 minutes, mice were perfused with 5 mL of 4% v/v paraformaldehyde. The aorta was removed and embedded in an 80-mm Petri dish containing 0.8% p/v high-grade, 245 low-melting-point agarose.

Two sets of images of the same aortas were acquired. The first set of images was taken with a fluorescent ultramicroscope (light sheet imaging macroscopy; LaVision Biotech, France), equipped with a light cube for Alexa Fluor 647 acquisition. For the second set of images, aortas were imaged with 2 different confocal microscopes. The first was a Leica TCS SP8 mounted on an upright stand DM6 FS (Leica Microsystems, Mannheim, Germany) equipped with 405, 488, 552, and 638 lasers. The scanning was done using a conventional scanner (10–1800 Hz). The microscope was equipped with a galvanometric stage to do fast z acquisition and a motorized xy stage.

Then, a more resolutive confocal microscope was used (a Leica TCS SP5 on an upright stand DM6000 (Leica Microsystems), controlled by the software LAS AF and using objective HC PL FLUOTAR 10× dry NA 0.30). The fluorescent molecule was excited with a laser Helium-Neon 633 nm, and the emission of fluorescence was collected on a conventional Photomultiplier Tube (PMT) from 650 to 720 nm. The transmitted light image was done at the same time on a PMT on transmission pathway. The 3-dimensional mosaic was done automatically on 4×2 positions by using the Tile Scan module included in the software controlling the motorized stage (Märzhäuser, Wetzlar, Germany). Finally, a maximum intensity projection was applied to represent the localization of the fluorescence signal through the thickness of the aorta.

The microscopy experiments were performed at the Bordeaux Imaging Center of the Neurosciences Institute of the University of Bordeaux, France.

Image Quantification

Immunofluorescence Image Quantification

Image processing and analysis were done automatically with a Fiji-ImageJ macro.[19] After opening the images from the ndpis source file with the Bio-formats plugin, a median filter was applied to remove noise. Then, for each tissue section, a different automatic threshold was applied for the red (P3 scFv-Fc) and green (mouse anti-galectin-3 and rabbit anti-LOX1 antibodies) channels to measure the area of positive pixels. Then, a logical AND was applied to create the colocalization image from the 2 separated channels and to determine the percentage of colocalization.

Ex Vivo Fluorescence Image Quantification

Image processing and analysis were done automatically with a Fiji-ImageJ macro.[19] After applying a median filter to remove noise, the tissue contour was automatically drawn using an automatic threshold in a brightfield image. This contour was then transferred to the fluorescence image (P3 scFv-Fc-2c or IgG antibodies) to measure the intensity of all the pixels inside the contour and the intensity of the pixels above a fixed threshold.

Statistical Analysis

All ELISA measurements were performed in triplicate and repeated in 3 independent experiments. Triplicate values were averaged, and differential analyses were then conducted using the Kruskal-Wallis methodology. The Dunn test method was then used to identify significant difference between proteins. Analyses were performed using the R environment (R Foundation for Statistical Computing, Vienna, Austria).

RESULTS

In Vivo Selection and Individual Screening by Flow Cytometry of scFv-Phages and Reformatting Into scFv-Fc Fragments

After the third round of in vivo biopanning of the MG-Umab library, >800 different scFv-phages were

Downloaded from http://ahajournals.org by on October 1, 2021

screened using protein extracts from rabbit atherosclerotic lesions. Overall, ≈200 scFv-phages (24%) recognized the atherosclerotic protein extracts (binding at least 2-fold above the background noise of wild-type phages) in flow cytometry experiments. Figure 1A and 1B show the results of a typical experiment with 4 positive scFv-phages (P3, D4, C8, and C4). The E9 clone was chosen as a negative control for all of the experiments. The gating strategy to analyze the binding of scFv-phages and scFv-Fc clones on rabbit atheromatous proteins coupled to beads is illustrated in Figure 1A.

On the basis of the immunohistochemistry results in rabbit aorta sections with atheromatous lesions and the antibody sequence integrity, 142 scFv-phages were finally considered for further investigation. Fifty of them were successfully produced in HEK-293 FreeStyle cells as soluble scFv-Fc fragments with a concentration >5 µg/mL (ie, threshold value for screening tests in supernatants). After scFv-Fc engineering, analysis of the antibody reactivity in supernatants by flow cytometry using protein extracts from rabbit atherosclerotic lesions[6] (Figure 1C) showed that 60% of the selected scFv-Fc maintained their reactivity.

In Vitro Validation of the Bioreactivity of Reformatted Clones by Immunohistochemistry Assays

ScFv-Fc capacity to recognize their targets in artery sections with atheromatous lesions from different mammalian species was assessed, as done for scFv-phages.[6] Figure 2 shows the results obtained with the P3, C4, D4, and C8 scFv-Fc antibodies. In sections of human endarterectomy specimens, the P3 scFv-Fc signal was strong in clusters of foam cells (arrowheads) and in areas with a necrotic core. In aorta sections from hypercholesterolemic rabbits, P3 staining was observed in the adventitia (A), in the intima (I) subendothelial area, and in some spindle-shaped cells in the disorganized media layer (M). In sections from *Apoe*$^{-/-}$ mouse aorta with atheroma plaques, the necrotic area (arrowhead) and adventitia (A) were clearly stained. In sections of the human endarterectomy sample, the C4 scFv-Fc antibody detected foam cells in necrotic cores of the subendothelial area and near to the tunica media (M) layer (arrowhead). Similarly, in atherosclerotic rabbit sections, specific C4 labeling was observed near the tunica media/intima (M/I) interface and in the necrotic core (arrowhead). In *Apoe*$^{-/-}$ mouse aorta sections, C4 scFv-Fc recognized the tunica intima (I) (arrowhead), although some unspecific background signal was observed because of degradation and detachment of the adventitia tissue on the slide (asterisks). D4 scFv-Fc only labeled a few groups of cells (arrowhead) in the atheroma plaque of the human carotid specimen. However, this signal might not be specific when compared with the background signal obtained by incubation with only the secondary antibody (upper panel, horseradish peroxidase-goat anti-human Fcγ). This is because of the presence of human antibodies in the plaque, despite the different specific blocking steps with goat serum, F(ab′)2 fragment goat anti-human IgG (H+L), and goat anti-human IgG (Fcγ specific). Conversely, in rabbit aorta sections, D4 scFv-Fc clearly labeled the intima (I) and the endothelium (arrowhead). In the *Apoe*$^{-/-}$ mouse aorta section, D4 scFv-Fc only labeled the adventitia (A) (arrowhead). C8 scFv-Fc did not show any significant labeling in all section types, with the exception of an area close to the tunica media (M, arrowhead) in rabbit aorta sections with atheromatous lesions, and the adventitia (A) in *Apoe*$^{-/-}$ mouse atheroma sections (arrowhead). Because the final aim of the study was to use in vivo–selected human antibodies as targeting moieties for the detection of atheromatous plaques in patients, the best translatable scFv-Fc antibodies were clearly P3 and C4, which displayed strong labeling of atheroma plaques in both animal models and also in human carotid sections. Moreover, the sequence of P3 was chosen as the reference for a recently published third-generation sequencing project to study clone enrichment during the in vivo phage display selection.[7] Specifically, it was among the best enriched sequences, and clones belonging to the same P3 clonotype with well-characterized somatic mutations in the VL gene were identified. On the basis of these previous results and because P3 reformatted as scFv-Fc showed the highest binding by flow cytometry and immunohistochemistry experiments, the rest of the study focused on the identification of the P3 scFv-Fc target, and C4 scFv-Fc was used as a comparison in LC-MS/MS analyses.

Antigen Identification by Immunoprecipitation and Proteomic Analyses

To identify the antigen recognized by P3 scFv-Fc among the proteins extracted from endarterectomy specimens, after immunoprecipitation of human endarterectomy proteins with the P3 and C4 scFv-Fc clones (P3-PH [proteins from human biopsies], C4-PH), samples were separated by SDS-PAGE followed by silver staining to visualize the major bands. In samples immunoprecipitated with P3 scFv-Fc, a single band with a relative molecular mass of 60 kDa was observed on the SDS-PAGE gel (Figure 3, SDS-PAGE 1). Conversely, after immunoprecipitation with C4 scFv-Fc, multiple bands were detected (Figure 3, SDS-PAGE 2). Extraction and analysis by LC-MS/MS of the different bands (Table S1) showed that in both cases, the most represented proteins in the MS/MS spectra

Downloaded from http://ahajournals.org by on October 1, 2021

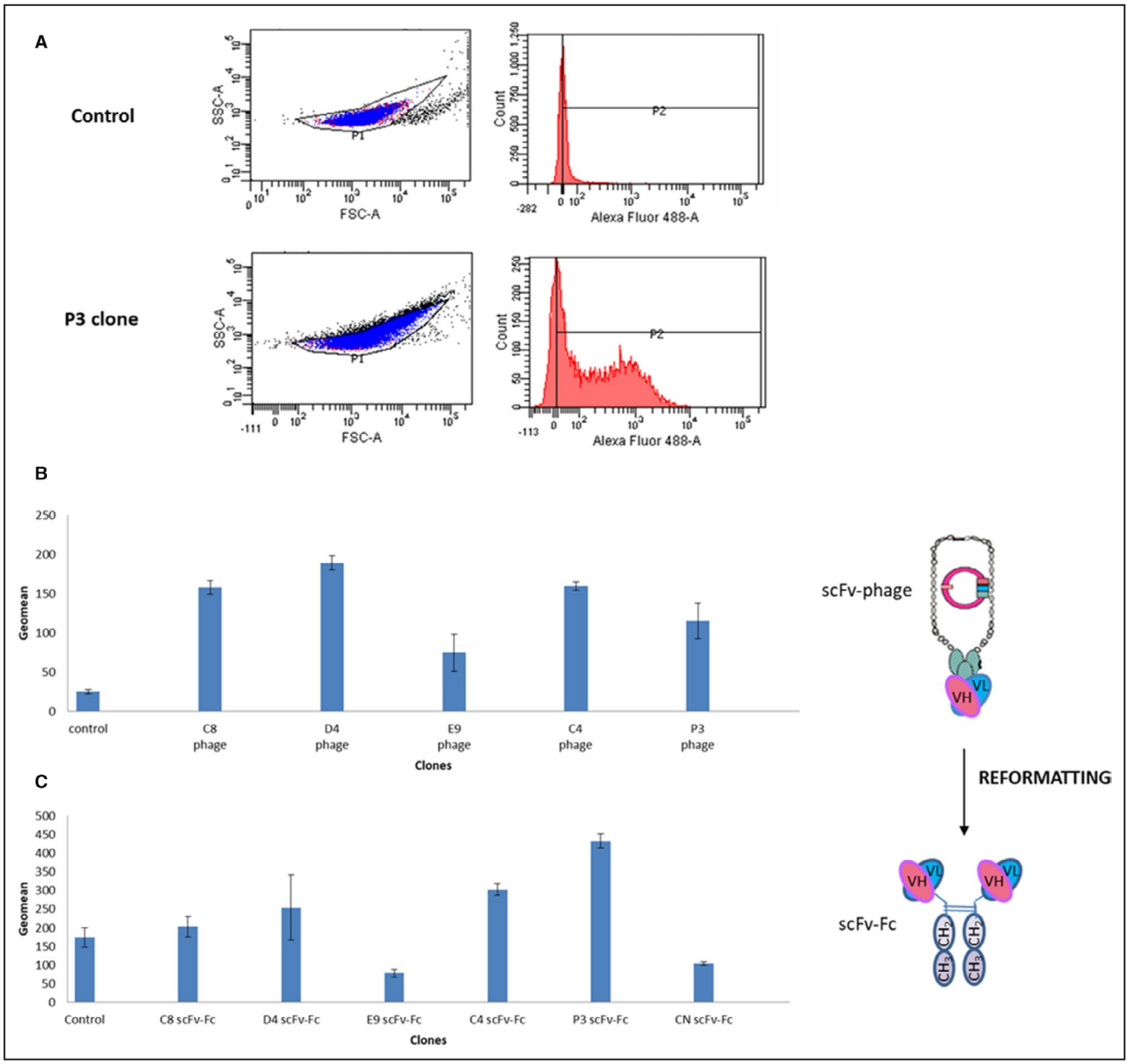


Figure 1. Flow cytometry analyses. A, Example of gating strategy to analyze the binding of scFv (single-chain fragment variable)-phages on rabbit atheromatous proteins coupled to beads.
The control (mouse anti-pVIII and Alexa Fluor 488–conjugated anti-mouse antibodies) and the P3 clone are illustrated. Binding of scFv-phages (**B**) and soluble scFv-Fc (single-chain fragment variable fused to the crystallizable fragment of immunoglobulin G) (**C**) on rabbit atheromatous proteins coupled to beads. Protein binding was detected using a mouse anti-pVIII antibody and an Alexa Fluor 488-conjugated anti-mouse antibody for scFv-phages, and using a rabbit anti-human Fc antibody and an Alexa Fluor 488–conjugated anti-rabbit antibody for scFv-Fc. Mean values±SD were calculated using the geometric mean of fluorescence (P2 geomean) obtained with 3 different antibody batches. The error bars represent the mean values±SD. CN indicates control negative; FSC-A,forward scatter area; VH, variable heavy; VL, variable light domains.

were keratin, filamin, vimentin, desmoglein, desmoplakin, and junction plakoglobin. However, galectin-3, a new biomarker of atherosclerosis,[20,21] was the highest represented protein in the P3-PH sample compared with C4-PH extract (abundance=35 326 405 in P3-PH and 1 266 731 in C4-PH; C4-PH/P3-PH abundance ratio=0.037 (Table S1). Because monomeric galectin-3 is subject to modifications, such as self-association (dimerization or oligomerization), which increase its range of biological activity,[22] this might explain the band detected at 60 kDa (theoretical molecular weight of galectin-3=30 kDa). To test this hypothesis, Gal3R was immunoprecipitated with a commercial anti-Gal3 Ab, and the immunoprecipitate (Gal3 Ab-Gal3R) was separated by SDS-PAGE. As observed with P3 scFv-Fc, a single band was detected (Figure 3, SDS-PAGE 3).

Downloaded from http://ahajournals.org by on October 1, 2021

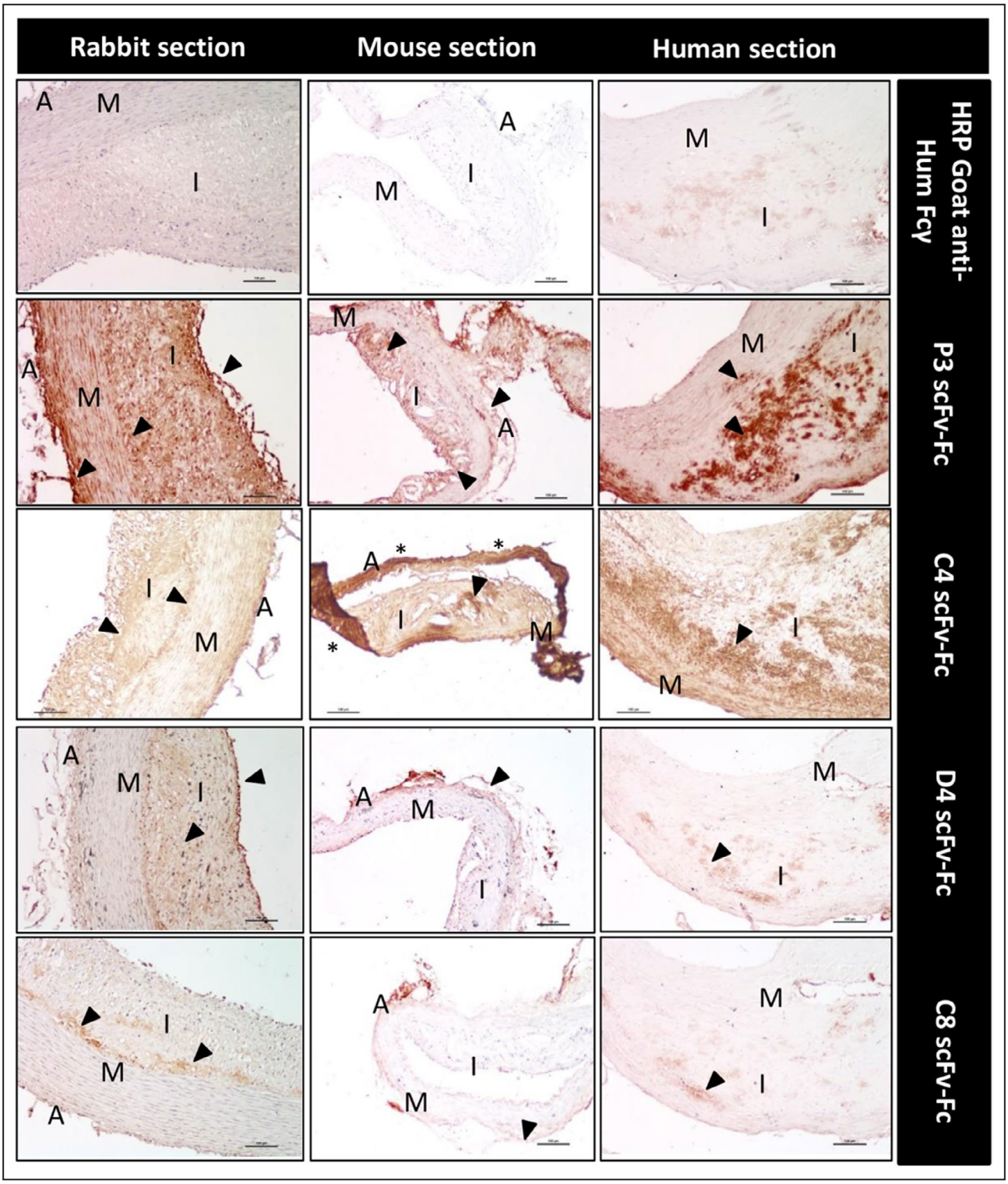


Figure 2. Immunohistochemical analysis of arterial tissue sections from atheromatous rabbits and *Apoe*$^{-/-}$ mice and human endarterectomy specimens using the indicated scFv-Fc (single-chain fragment variable fused to the crystallizable fragment of immunoglobulin G).

The different areas in transversal sections are identified: adventitia (A), media (M), and intima (I). Sections were incubated with the indicated scFv-Fc antibodies (P3, C4, D4, and C8), followed by the HRP-conjugated goat anti-human Fcγ antibody, and the DAB substrate kit reagent. The yellow-brown staining indicates the presence of the antigen recognized by the scFv-Fc. No staining was observed in mouse and rabbit sections incubated with the secondary antibody alone, and there is low background noise in the human sections (upper panels). Scale bars, 100 μm. Nuclei were counterstained with hematoxylin. DAB indicates 3,3′-diaminobenzidine; and HRP, horseradish peroxidase.

Downloaded from http://ahajournals.org by on October 1, 2021

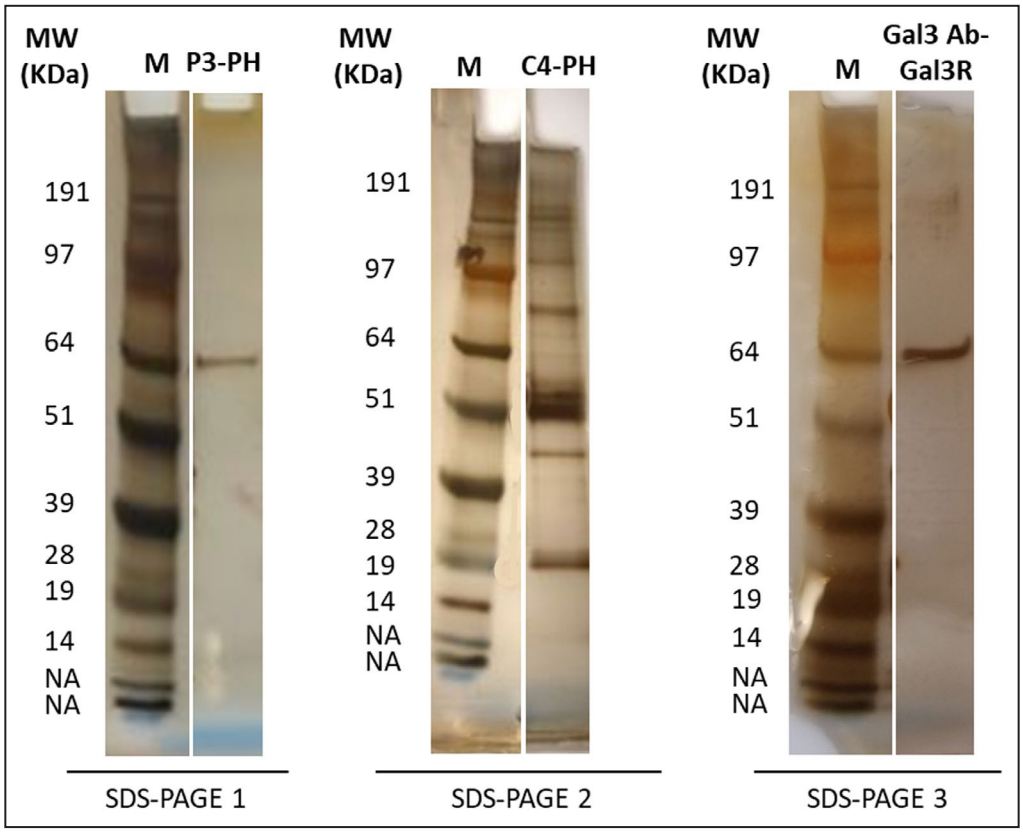


Figure 3. SDS-PAGE analysis of immune complexes.
After immunoprecipitate elution in 2×SDS Laemmli buffer, immune complexes were separated on polyacrylamide gels (4%–10%) and stained with silver nitrate. SDS-PAGE 1 and 2: proteins extracted from human endarterectomy specimens were immunoprecipitated with the P3 and C4 scFv-Fc (single-chain fragment variable fused to the crystallizable fragment of immunoglobulin G) (from mammalian cells), respectively. SDS-PAGE 3: Gal3R (recombinant galectin-3 protein) was immunoprecipitated with a commercial anti-GAL3 Ab (anti-galectin-3 antibody). MW indicates molecular weight; M, marker; NA, non attributed; PH, proteins from human biopsies.

Moreover, the Gal3R protein was identified by LC-MS/MS analysis for the Gal3 Ab-Gal3R immunoprecipitate, with an abundance of 30 552 241. Comparison of galectin-3 abundance in Gal3Ab-Gal3R and P3-PH gave a ratio close to 1 (Gal3Ab-Gal3R/P3-PH ratio=0.739), indicating a comparable galectin-3 amount in the 2 immunoprecipitates (Table S1).

Then, to assess the specificity of P3 scFv-Fc binding to galectin-3, an ELISA assay was performed using recombinant galectin-3 and galectin-3BP proteins, which is the main galectin-3 ligand,[23] and also recombinant galectin-1, another β-galactoside lectin family member, and other irrelevant proteins such as BSA and the GPαIIbβ3 integrin (Figure 4A). Globally, average OD values tended to significantly differ ($P_{Kruskas\text{-}Wallis}$=0.0503) between studied proteins. Deeper analyses revealed that OD was significantly higher in galectin-3 than in galectin-3BP (P=0.022), BSA (P=0.018), and galectin-1 (P=0.002) (Figure 4A). These results highlight that P3 scFv-Fc bound specifically to galectin-3, and did not recognize galectin-3BP, galectin-1 protein, and BSA. Some cross-reactivity was observed with GPαIIbβ3, with a P value=0.1087 for galectin-3 versus GPαIIbβ3. This could be explained by the fact that integrins, such as GPα3β1[24] and GPαvβ3,[25] are among the galectin-3 ligands. Commercial antibodies against all these recombinant proteins and the AP2 (AP2 clone) antibody were used as positive controls, and the irrelevant CN antibody (scFv-Fc format) as a negative control (Figure 4B).

To further validate the identified target in human endarterectomy samples, immunofluorescence experiments were performed with P3 scFv-Fc and a commercial murine antibody against human galectin-3. Image analysis (Figure 5A through 5D) showed that P3 scFv-Fc labeled tunica intima areas that were recognized also by the commercial anti-galectin-3 antibody as indicated by the enlarged merge image (64.62% of colocalization with the commercial anti-galectin-3 antibody) (Figure 5C).

Downloaded from http://ahajournals.org by on October 1, 2021

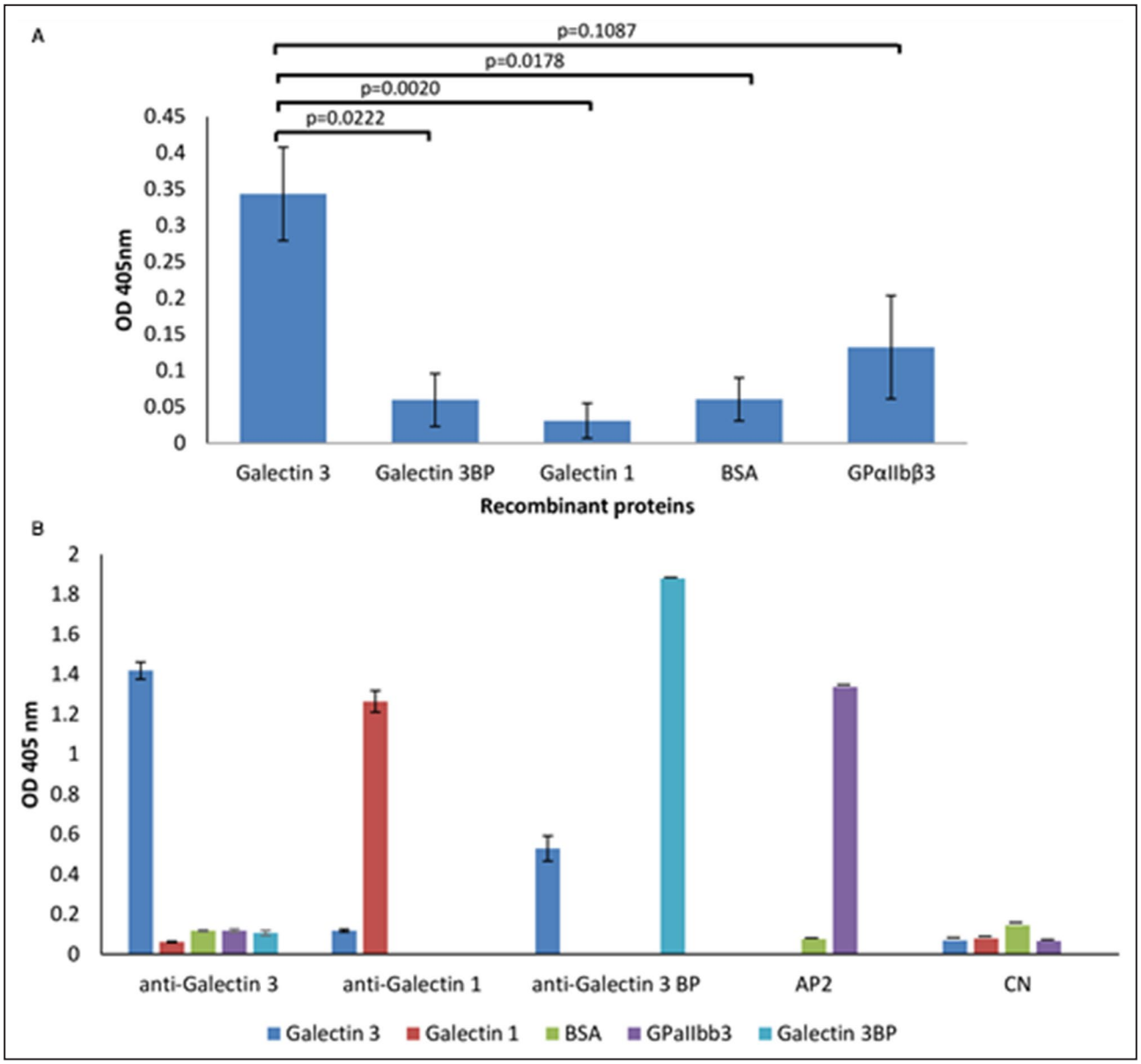


Figure 4. Binding of P3 scFv-Fc (single-chain fragment variable fused to the crystallizable fragment of immunoglobulin G) and control antibodies to recombinant proteins by ELISA assay.

A, P3 scFv-Fc showed stronger binding to recombinant galectin-3 than to the galectin-3BP (galectin-3 binding protein) ligand. Galectin-1 and Glycoprotein αIIbβ3 (GPαIIbβ3) were used to assess the specificity of galectin-3 binding. An irrelevant antigen (BSA) served as a negative control. P3 scFv-Fc binding was detected with a horseradish peroxidase (HRP)-conjugated anti-human Fcγ antibody, and absorbance was measured at 405 nm. Data are the means of 3 independent experiments repeated in triplicate. According to the Kruskal-Wallis test followed by the Dunn test, differential analyses provided the following *P* values: *P*=0.0222 for galectin-3 vs galectin-3BP, *P*=0.0020 for galectin-3 vs galectin-1, *P*=0.0178 for galectin-3 vs BSA, and *P*=0.1087 for galectin-3 vs GPαIIbβ3. **B**, The specificity of the commercial antibodies against galectin-3, galectin-1, and galectin-3BP, of the mouse AP2 (AP2 clone) antibody (from Dr Nurden) against GPαIIbβ3 integrin, and of CN (control negative) scFv-Fc (negative control; from Laboratoire Français de Fractionnement et de Biotechnologies) was assesses by ELISA with recombinant galectin-3, galectin-1, galectin-3BP, BSA, and GPαIIbβ3. The anti-galectin-3 and anti-galectin-3BP antibodies were detected with an HRP-conjugated anti-rabbit antibody. The galectin-1 and AP2 antibodies were detected with an HRP-conjugated anti-mouse antibody. CN was detected with a peroxidase-conjugated anti-human FCγ antibody. The error bars reprement the mean values±SD.

Because galectin-3 is overexpressed by macrophages,[26] human coronary biopsies were analyzed using P3 scFv-Fc and a rabbit antibody against LOX1 (the macrophage receptor for oxidized LDL) (Figure 5E through 5H). The enlarged merge image shows the colocation between P3 scFv-Fc and LOX1, especially in the subendothelial and lipid core areas (79.31%) (Figure 5G). Because galectin-3 is expressed also by

Downloaded from http://ahajournals.org by on October 1, 2021

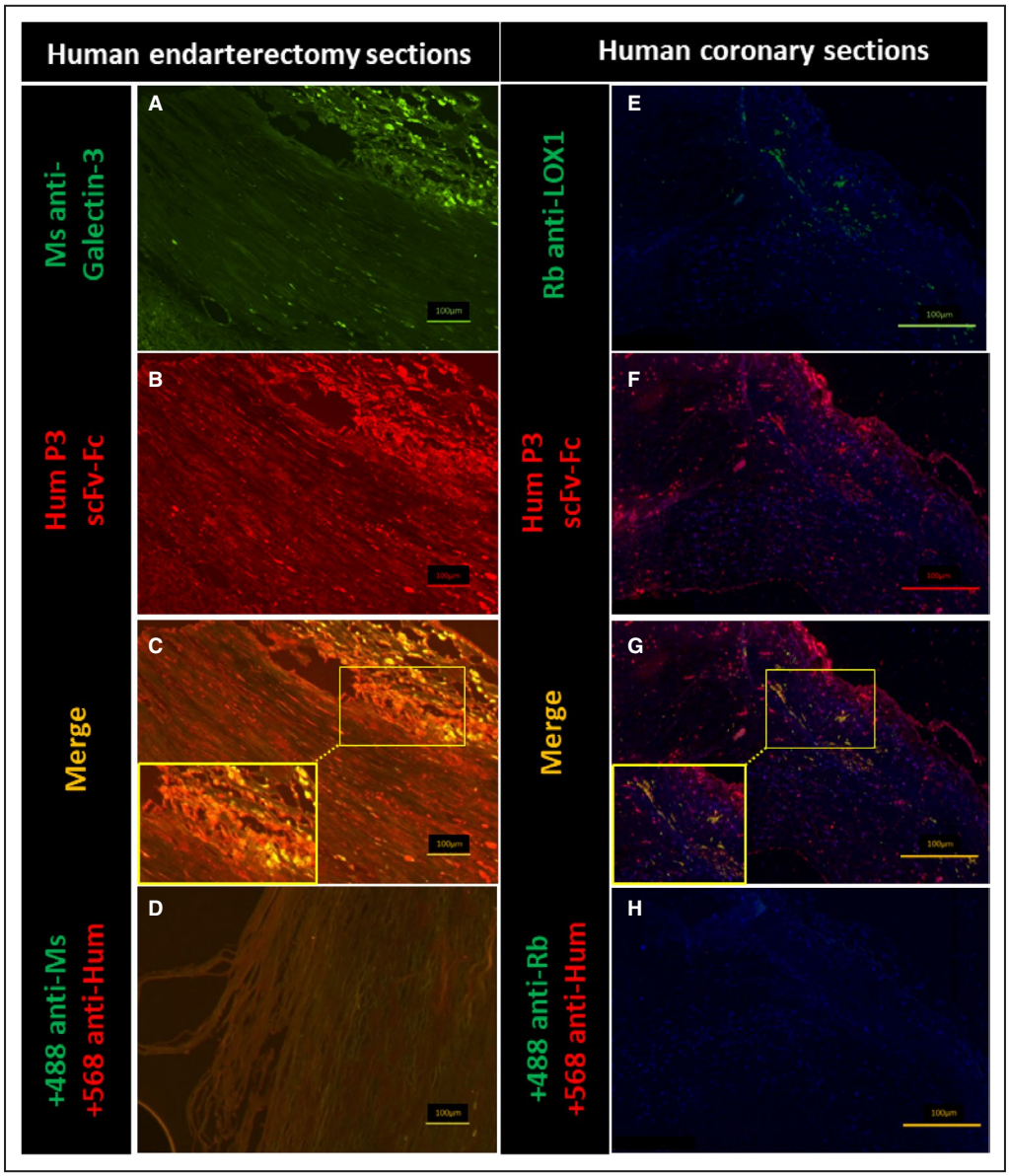


Figure 5. Colocalization of P3 scFv-Fc (single-chain fragment variable fused to the crystallizable fragment of immunoglobulin G) with an anti-galectin-3 antibody and an anti-LOX1 (lectin-type oxidized LDL receptor 1) antibody in the intima of human endarterectomy specimens and coronary sections.

A through **D**, Co-staining of P3 scFv-Fc (single-chain fragment variable fused to the crystallizable fragment of immunoglobulin G) and an anti-galectin-3 antibody in human endarterectomy sections by immunofluorescence. An Alexa Fluor 488 anti-mouse antibody (+488 anti-Ms [mouse]) was used to reveal the specific binding of the commercial anti-human galectin-3 antibody (Ms anti-galectin-3) (**A** and **C**). The Alexa Fluor 568 anti-human antibody (+568 anti-Hum) was used to reveal the specific binding of P3 scFv-Fc (Hum P3 scFv-Fc) (**B** and **C**). Before image merging, the red and green fluorescence signals were adjusted to comparable levels. The yellow color indicates colocalization of the antigens recognized by P3 scFv-Fc and the anti-human galectin-3 antibody (**C**). Secondary antibodies alone were used as negative controls (**D**). Size bars: 100 μm. **E** through **H**, The Alexa Fluor 488 anti-rabbit antibody (+488 anti-Rb [rabbit]) was used to reveal the specific binding of the commercial anti-LOX1 antibody (Rb anti-LOX1) (**E** and **G**). The Alexa Fluor 647 anti-human antibody (+568 anti-Hum) was used to reveal the specific binding of P3-scFv-Fc (Hum P3 scFv-Fc) (**F** and **G**). Before image merging, the red and green fluorescence signals were adjusted to comparable levels. The yellow color indicates colocalization of the antigens labeled by P3 scFV-Fc and anti-LOX1 antibody (**G**). As galectin-3 is also expressed also by other cell types (ie, mast cells, eosinophils, neutrophils, endothelial cells, and activated T and B cells[8,27]), areas outside the macrophage location also are stained by P3 scFv-Fc (**G**). Size bars: 100 μm.

Downloaded from http://ahajournals.org by on October 1, 2021

other cell types (eg, mast cells, eosinophils, neutrophils, endothelial cells, and activated T and B cells),[8,27] areas outside the macrophage location were also stained by P3 scFv-Fc (Figure 5F and 5G).

P3 ScFv-Fc Labels Atheroma Plaques in *Apoe*$^{-/-}$ Mice

To assess whether P3 scFv-Fc could be used for atheroma diagnostic imaging, first we costained aorta sections from *Apoe*$^{-/-}$ mice (a model of atherosclerosis) with P3 scFv-Fc and the anti-LOX1 antibody (Figure 6). The colocalization (in yellow) of the P3 scFv-Fc and anti-LOX1 antibodies (84.24%) indicated the presence of galectin-3 in the area of foam cells. Next, the P3 scFv-Fc binding profile was characterized ex vivo in the aorta of *Apoe*$^{-/-}$ and wild-type mice (Figure 7 and Figure S1). For this experiment, the P3 antibody with 2 extra cysteines at the C-terminus (P3 scFv-Fc-2c) was used. This modification is crucial for coupling the antibody to nanoparticles in future magnetic resonance imaging experiments. P3 scFv-Fc-2c specificity was assessed and validated by flow cytometry (data not shown). Compared with the signal obtained from control human IgG in *Apoe*$^{-/-}$ mouse aorta, macroscale fluorescence imaging revealed a significant signal of P3 scFv-Fc-2c in the aortic root (83.33%) (yellow arrowheads in Figure 7). Conversely, P3 scFv-Fc-2c and the human IgG control did not give any significant signal in the aorta of wild-type mice.

In addition to this first set of images, the specific binding of P3 scFv-Fc-2c on atheromatous plaques was confirmed by the confocal microcopy images shown in Figure S1 (yellow arrowheads, Figure S1B and S1F).

DISCUSSION

Nowadays, there is a rising interest in accessing and characterizing the molecular and cellular components of atheroma plaques to find strategies for reducing the associated risk of stroke and myocardial infarction. It is acknowledged that the plaque composition more than the narrowing of arteries defines the condition of plaque rupture. Imaging technologies are frequently used to determine the molecular composition of atheroma plaques, and specific contrast agents are urgently needed. This specificity can be offered by human antibodies that can target atherosclerosis biomarkers for diagnostic purposes.

Phage display is an efficient tool for biomarker identification for several tissues and cell types. Keller et al

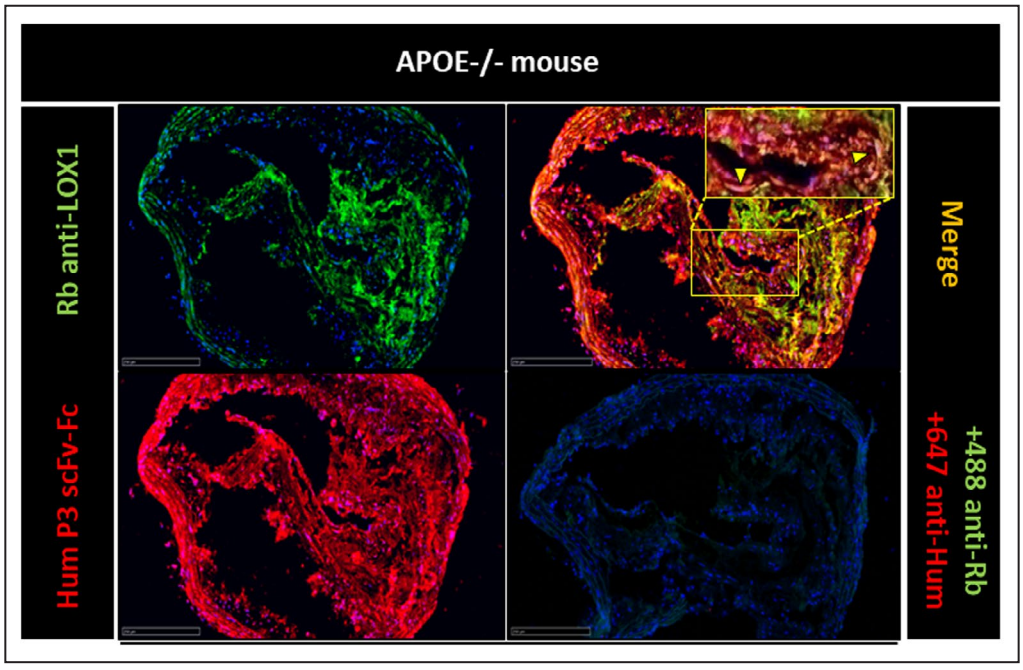


Figure 6. In vitro immunofluorescence analysis of *Apoe*$^{-/-}$ aorta sections with P3 scFv-Fc (single-chain fragment variable fused to the crystallizable fragment of immunoglobulin G) and an anti-LOX1 (lectin-type oxidized LDL receptor 1) antibody.
Colocalization analysis by fluorescence microscopy in *Apoe*$^{-/-}$ mouse aorta sections of the antigens recognized by P3 scFv-Fc and the commercial anti-LOX1 antibody. The Alexa Fluor 488 anti-rabbit antibody (+488 anti-Rb) was used to reveal the specific binding of the anti-LOX1 antibody (Rb anti-LOX1). The Alexa Fluor 647 anti-human antibody (+647 anti-Hum) was used to reveal the specific binding of P3 scFv-Fc (Hum P3 scFv-Fc). Before image merging, the red and green fluorescence signals were adjusted to comparable levels. The yellow color and yellow arrowheads indicate colocalization of the antigens recognized by P3 scFv-Fc and the anti-LOX1 antibody. Size bars: 250 μm.

Downloaded from http://ahajournals.org by on October 1, 2021

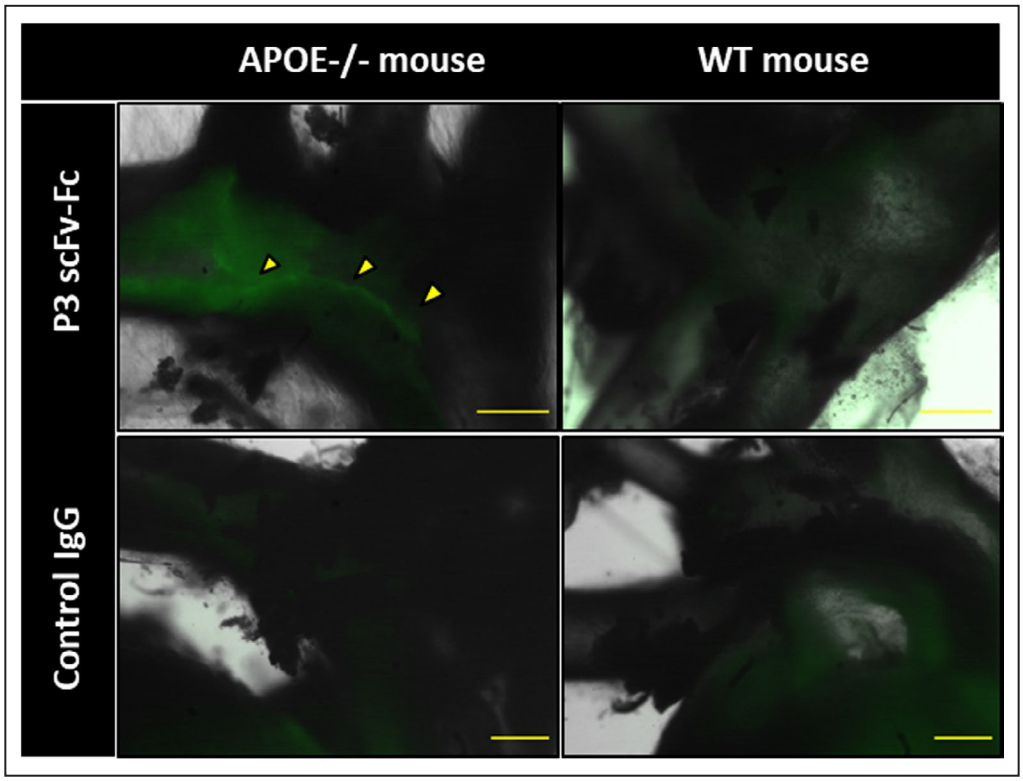


Figure 7. Ex vivo imaging of P3 scFv-Fc (single-chain fragment variable fused to the crystallizable fragment of immunoglobulin G) in *Apoe*$^{-/-}$ and wild-type (WT) mice using a fluorescent ultramicroscope.

Fluorescence macroscopy analysis of P3 scFv-Fc coupled to Alexa Fluor 568 dye after ex vivo injection in *Apoe*$^{-/-}$ and WT mice. A human immunoglobulin (Ig)G coupled to Alexa Fluor 568 was used as negative control antibody. P3 scFv-Fc shows specific labeling of the atheroma in the *Apoe*$^{-/-}$ mouse (yellow arrowheads). Size bars: 500 μm.

developed the direct cell phage display approach to select human scFv that targets blood and lymphatic cells in cancer.[28] In atherosclerosis, the combination of this method and fresh human tissues allowed the selection of peptides against CD100.[29]

In 1998, Arap et al set up the first in vivo phage display method to map endothelial cells in cancer.[30] Later on, Arap et al,[31] Staquicini et al,[32] and Krag et al[33] initiated a human vascular mapping project and identified peptides that recognize tumor cells in patients with cancer. In atherosclerosis, in vivo phage selection in animal models led to the discovery of peptides[34] and antibodies[35,36] that bind to a large panel of targets in their microenvironment, thus allowing studying the atheroma plaque composition. One important limitation of in vivo phage display using antibody fragments is the identification of the target among all of the overexpressed proteins extracted from tissues. Unlike peptides that can be compared with protein databases,[32] in vivo antibody discovery requires more complex methodologies for target identification to better understand the pathogenesis and for biotherapeutic innovation. However, the myriad of unknown targets, which is a drawback of in vivo phage display using antibodies, also represents a large panel of antibody targets in their microenvironment. Here, immunoprecipitation and mass spectrometry analyses were used to show that galectin-3, a protein of 25 to 30 kDa, is the target of P3 scFv-Fc in proteins extracted from human endarterectomy samples.

Galectin-3 is a member of a family of 15 β-galactoside-binding proteins, named galectins, characterized by the presence of conserved carbohydrate recognition domains. Galectin-3 is the only chimera-type galectin in vertebrates, with a single carbohydrate recognition domain and a nonlectin N-terminal domain. Galectins are synthesized in the cytoplasm and secreted through a nonclassical exocytic pathway[37] to interact with cell surface glycans. They regulate the immune system by modulating monocyte/macrophage functions.[38] Galectin-3 is implicated in different biological processes, including cell activation, anti-apoptotic activity, cytokine secretion, and cell migration.[22,39–42] Galectin-3 also strongly induces P-selectin, which interacts with PSGL1 (P-selectin glycoprotein ligand 1) on leukocyte to form platelet-leukocyte aggregates.[43] The

Downloaded from http://ahajournals.org by on October 1, 2021

interaction between platelets and leukocytes promotes their activation, which is crucial for triggering inflammation, vascular remodeling, and thrombosis. Galectin-3 implication in different processes in cancer[44–47] and inflammation led to the development of molecules to block the underlying mechanisms.[48]

Currently, much interest is focused on the role of galectin-3 in cardiovascular diseases, particularly in atherosclerosis.[20,24,42,49–51] Galectin-3 protein was first detected in carotid samples from endarterectomies.[26] Galectin-3 has been considered as an inflammation amplifier during atherosclerotic plaque progression[10] because of its close interrelation with macrophages and foam cells. Zhu et al showed that ^{125}I-oxidized LDL and ^{125}I-acetylated LDL are actively endocytosed by galectin-3-expressing chinese hamster ovary (CHO) cells. Moreover, incubation with acetylated-LDL led to intracellular accumulation of cholesteryl esters, highlighting galectin-3 role in endocytosis of advanced glycation end-proteins and modified LDLs.[52] More recently, Madrigal-Matute et al reported that galectin-3 can modulate oxidative stress by stimulating superoxide production in monocytes and regulates the adhesion of monocytes/macrophages to endothelial cells.[50] Because of its implication in various diseases, galectin-3 therapeutic potential has been evaluated using inhibitors and animal knock-out models.[53] In atherosclerosis, inactivation of *Lgals3* (the gene encoding galectin-3) in *Apoe*$^{-/-}$ mice reduces the atheroma thickness.[54,55] Moreover, in patients on chronic statin treatment, galectin-3 level was elevated, and the macrophage number was reduced within plaques, suggesting that this protein is a biomarker of plaque inflammation severity.[56] Dysfunction of the endothelial barrier is the starting point of atherosclerosis; however, the exact role of galectin-3 in endothelial cells is unclear. A recent study showed that the interaction between galectin-3 and integrin β1 promotes different inflammatory factors, leading to endothelial cell stress and apoptosis.[57] Galectin-3 might have both pro- and antiatherosclerotic roles. For instance, increased accumulation of galectin-3–negative macrophages has been observed in advanced human, rabbit, and mouse plaques compared with early lesions.[58] Although many studies reported high galectin-3 expression in plaque macrophages, the functional heterogeneity of the macrophage population needs to be taken into account when assessing galectin-3 expression. Single-cell technologies, such as single-cell RNA sequencing and cytometry by time-of-flight, allowed identifying different macrophage clusters with different gene expression profiles and phenotypes. Besides the resident-like and proinflammatory subsets, the newly described anti-inflammatory TREM2^{hi} macrophages display enrichment in lipid metabolism, cholesterol efflux, oxidative phosphorylation, and catabolism, and also strongly express galectin-3.[59–61] The TREM2^{hi} subset of macrophages has been linked to lipid uptake and foam cell formation,[62] which are mainly associated with plaque progression. However, in agreement with the recent publication by Di Gregoli et al[58] emphasizing that galectin-3 identifies a subset of macrophages with a beneficial role in plaque regression, the gene expression profile of foamy macrophages was also associated with plaque-resolving parameters, such as efferocytosis and tissue repair.[62]

Moreover, during atherosclerosis progression, foamy macrophage apoptosis may contribute to disease worsening. Although in the present study we did not compare plaque composition and phenotype in early and advanced atherosclerotic lesions in animal models and in human samples, we did observe significant differences in galectin-3 expression in human samples (data not shown). Additional analyses of macrophages from plaques at different disease stages would be useful to characterize galectin-3 expression level in nonfoamy, foamy, and apoptotic macrophages and to determine whether our anti-galectin-3 antibody P3 scFv-Fc could be used as a marker of plaque stability or progression.

All of these studies indicate that galectin-3 is an ideal target for imaging modalities and for developing biotherapeutics to regulate its role in atherosclerosis by directly targeting this protein or one of its ligands (eg, galectin-3 binding protein,[63] integrins GPα3β1,[24] and GPαvβ3[25]), which are all overexpressed in atherosclerosis. Because P3 scFv-Fc can bind to galectin-3 ex vivo, future studies should determine whether this antibody can act as an antagonist or agonist on one of the mechanisms implicated in the inflammation process that characterizes atherosclerosis. If necessary, random mutations could be introduced in P3 scFv-Fc using human polymerases[5,64] to increase its affinity for galectin-3. Moreover, our recent study performed by third-generation sequencing of scFv clones issued from the in vivo selection[7] highlighted sequences related to the P3 scFv clone with point mutations.

In conclusion, our study shows that the combination of in vivo antibody selection and in vitro characterization of the target by considering the pathological microenvironment is a good starting point for developing diagnostic and biotherapeutic molecules that can easily be transferred to the clinic.

ARTICLE INFORMATION

Received April 14, 2020; accepted March 10, 2021.

Affiliations

CRMSB (Centre de Resonance Magnétique des Systèmes Biologiques), UMR5536 CNRS (Centre National de Recherche Scientifique), INSB (Institut National des Sciences Biologiques), Bordeaux, France (A.H., J.L., F.O., S.S., S.M., C.L., G.C.-S, M.-J.J.-V.); LFB (Laboratoire Français de Fractionnement et de Biotechnologies) Biotechnologies, Lille, France (A.F., P.M.); Protéome

Downloaded from http://ahajournals.org by on October 1, 2021

Pole, CGFB (Centre de Génomique Fonctionnelle de Bordeaux), Bordeaux, France (S.C.); CHU Pellegrin, Bordeaux, France (É.D.); UPS3044, CNRS (Centre National de Recherche Scientifique), Saint-Christol-Lès-Alès, France (M.D.-C.); and BE4S (Bio-Experts for Success), Croix, France (A.F.).

Acknowledgments

The microscopy work was done at Bordeaux Imaging Center, a service unit of CNRS-INSERM and Bordeaux University, a member of the national France BioImaging infrastructure supported by the French National Research Agency (ANR-10-INBS-04). The help of C. Poujol and S. Marais is acknowledged. The statistical analysis was done by D.-A. Tregouet, Centre Bordeaux Population Research, Inserm U1219.

Sources of Funding

This work was supported by grant ANR-13-BSV5-0018 from the French National Research Agency Program named ATHERANOS and a public grant from the French National Research Agency in the context of the Investments for the Future Program, reference ANR-10-LABX-57 named TRAIL and ANR-10-LABX-53 named MabImprove.

Disclosures

None.

Supplementary Material

Table S1
Figure S1

REFERENCES

1. Hansson GK, Libby P. The immune response in atherosclerosis: a double-edged sword. *Nat Rev Immunol*. 2006;6:508–519.
2. Virmani R, Kolodgie FD, Burke AP, Farb A, Schwartz SM. Lessons from sudden coronary death: a comprehensive morphological classification scheme for atherosclerotic lesions. *Arterioscler Thromb Vasc Biol*. 2000;20:1262–1275. DOI: 10.1161/01.ATV.20.5.1262.
3. Kunjathoor VV, Febbraio M, Podrez EA, Moore KJ, Andersson L, Koehn S, Rhee JS, Silverstein R, Hoff HF, Freeman MW. Scavenger receptors class A-I/II and CD36 are the principal receptors responsible for the uptake of modified low density lipoprotein leading to lipid loading in macrophages. *J Biol Chem*. 2002;277:49982–49988. DOI: 10.1074/jbc.M209649200.
4. Lariviere M, Lorenzato CS, Adumeau L, Bonnet S, Hemadou A, Jacobin-Valat MJ, Noubhani A, Santarelli X, Minder L, Di Primo C, et al. Multimodal molecular imaging of atherosclerosis: nanoparticles functionalized with scFv fragments of an anti-alphaIIbbeta3 antibody. *Nanomed Nanotechnol Biol Med*. 2019;22: 102082.
5. Mondon P, Souyris N, Douchy L, Crozet F, Bouayadi K, Kharrat H. Method for generation of human hyperdiversified antibody fragment library. *Biotechnol J*. 2007;2:76–82. DOI: 10.1002/biot.200600205.
6. Hemadou A, Laroche-Traineau J, Antoine S, Mondon P, Fontayne A, Le Priol Y, Claverol S, Sanchez S, Cerutti M, Ottones F, et al. An innovative flow cytometry method to screen human scFv-phages selected by in vivo phage-display in an animal model of atherosclerosis. *Sci Rep*. 2018;8:15016. DOI: 10.1038/s41598-018-33382-2.
7. Hemadou A, Giudicelli V, Smith ML, Lefranc MP, Duroux P, Kossida S, Heiner C, Hepler NL, Kuijpers J, Groppi A, et al. Pacific biosciences sequencing and IMGT/HighV-QUEST analysis of full-length single chain fragment variable from an in vivo selected phage-display combinatorial library. *Front Immunol*. 2017;8:1796. DOI: 10.3389/fimmu.2017.01796.
8. Sciacchitano S, Lavra L, Morgante A, Ulivieri A, Magi F, De Francesco GP, Bellotti C, Salehi LB, Ricci A. Galectin-3: one molecule for an alphabet of diseases, from a to z. *Int J Mol Sci*. 2018;19. DOI: 10.3390/ijms19020379.
9. Papaspyridonos M, McNeill E, de Bono JP, Smith A, Burnand KG, Channon KM, Greaves DR. Galectin-3 is an amplifier of inflammation in atherosclerotic plaque progression through macrophage activation and monocyte chemoattraction. *Arterioscler Thromb Vasc Biol*. 2008;28:433–440. DOI: 10.1161/ATVBAHA.107.159160.
10. Novak R, Dabelic S, Dumic J. Galectin-1 and galectin-3 expression profiles in classically and alternatively activated human macrophages. *Biochim Biophys Acta*. 2012;1820:1383–1390. DOI: 10.1016/j.bbagen.2011.11.014.
11. Sano H, Hsu DK, Yu L, Apgar JR, Kuwabara I, Yamanaka T, Hirashima M, Liu FT. Human galectin-3 is a novel chemoattractant for monocytes and macrophages. *J Immunol*. 2000;165:2156–2164. DOI: 10.4049/jimmunol.165.4.2156.
12. Deramchia K, Jacobin-Valat MJ, Laroche-Traineau J, Bonetto S, Sanchez S, Dos Santos P, Massot P, Franconi JM, Martineau P, Clofent-Sanchez G. By-passing large screening experiments using sequencing as a tool to identify scFv fragments targeting atherosclerotic lesions in a novel in vivo phage display selection. *Int J Mol Sci*. 2012;13:6902–6923. DOI: 10.3390/ijms13066902.
13. Renaut L, Monnet C, Dubreuil O, Zaki O, Crozet F, Bouayadi K, Kharrat H, Mondon P. Affinity maturation of antibodies: optimized methods to generate high-quality ScFv libraries and isolate IgG candidates by high-throughput screening. *Methods Mol Biol (Clifton. NJ)*. 2012;907:451–461.
14. Alamyar E, Duroux P, Lefranc MP, Giudicelli V. IMGT((r)) tools for the nucleotide analysis of immunoglobulin (IG) and t cell receptor (TR) V-(D)-J repertoires, polymorphisms, and IG mutations: IMGT/V-QUEST and IMGT/HighV-QUEST for NGS. *Methods Mol Biol*. 2012;882:569–604.
15. Juliant S, Leveque M, Cerutti P, Ozil A, Choblet S, Violet ML, Slomianny MC, Harduin-Lepers A, Cerutti M. Engineering the baculovirus genome to produce galactosylated antibodies in lepidopteran cells. *Methods Mol Biol*. 2013;988:59–77.
16. Fessart D, Martin-Negrier ML, Claverol S, Thiolat ML, Crevel H, Toussaint C, Bonneu M, Muller B, Savineau JP, Delom F. Proteomic remodeling of proteasome in right heart failure. *J Mol Cell Cardiol*. 2014;66:41–52. DOI: 10.1016/j.yjmcc.2013.10.015.
17. Kall L, Canterbury JD, Weston J, Noble WS, MacCoss MJ. Semi-supervised learning for peptide identification from shotgun proteomics datasets. *Nat Methods*. 2007;4:923–925. DOI: 10.1038/nmeth1113.
18. Spivak M, Weston J, Bottou L, Kall L, Noble WS. Improvements to the percolator algorithm for peptide identification from shotgun proteomics data sets. *J Proteome Res*. 2009;8:3737–3745. DOI: 10.1021/pr800109k.
19. Schindelin J, Arganda-Carreras I, Frise E, Kaynig V, Longair M, Pietzsch T, Preibisch S, Rueden C, Saalfeld S, Schmid B, et al. Fiji: an open-source platform for biological-image analysis. *Nat Methods*. 2012;9:676–682. DOI: 10.1038/nmeth.2019.
20. Aksan G, Gedikli O, Keskin K, Nar G, Inci S, Yildiz SS, Kaplan O, Soylu K, Kilickesmez KO, Sahin M. Is galectin-3 a biomarker, a player-or both-in the presence of coronary atherosclerosis? *J Investig Med*. 2016;64:764–770. DOI: 10.1136/jim-2015-000041.
21. Falcone C, Lucibello S, Mazzucchelli I, Bozzini S, D'Angelo A, Schirinzi S, Totaro R, Falcone R, Bondesan M, Pelissero G. Galectin-3 plasma levels and coronary artery disease: a new possible biomarker of acute coronary syndrome. *Int J Immunopathol Pharmacol*. 2011;24:905–913. DOI: 10.1177/039463201102400409.
22. Suthahar N, Meijers WC, Sillje HHW, Ho JE, Liu FT, de Boer RA. Galectin-3 activation and inhibition in heart failure and cardiovascular disease: an update. *Theranostics*. 2018;8:593–609. DOI: 10.7150/thno.22196.
23. DeRoo EP, Wrobleski SK, Shea EM, Al-Khalil RK, Hawley AE, Henke PK, Myers DD Jr, Wakefield TW, Diaz JA. The role of galectin-3 and galectin-3-binding protein in venous thrombosis. *Blood*. 2015;125:1813–1821. DOI: 10.1182/blood-2014-04-569939.
24. van der Hoeven NW, Hollander MR, Yildirim C, Jansen MF, Teunissen PF, Horrevoets AJ, van der Pouw Kraan TC, van Royen N. The emerging role of galectins in cardiovascular disease. *Vascul Pharmacol*. 2016;81:31–41. DOI: 10.1016/j.vph.2016.02.006.
25. Markowska AI, Liu FT, Panjwani N. Galectin-3 is an important mediator of VEGF- and bFGF-mediated angiogenic response. *J Exp Med*. 2010;207:1981–1993. DOI: 10.1084/jem.20090121.
26. Nachtigal M, Al-Assaad Z, Mayer EP, Kim K, Monsigny M. Galectin-3 expression in human atherosclerotic lesions. *Am J Pathol*. 1998;152:1199–1208.
27. Liu FT. Regulatory roles of galectins in the immune response. *Int Arch Allergy Immunol*. 2005;136:385–400. DOI: 10.1159/000084545.
28. Keller T, Kalt R, Raab I, Schachner H, Mayrhofer C, Kerjaschki D, Hantusch B. Selection of scFv antibody fragments binding to human blood versus lymphatic endothelial surface antigens by direct cell phage display. *PLoS One*. 2015;10:e0127169. DOI: 10.1371/journal.pone.0127169.
29. Luque MC, Gutierrez PS, Debbas V, Martins WK, Puech-Leao P, Porto G, Coelho V, Boumsell L, Kalil J, Stolf B. Phage display identification of

Downloaded from http://ahajournals.org by on October 1, 2021

CD100 in human atherosclerotic plaque macrophages and foam cells. *PLoS One*. 2013;8:e75772. DOI: 10.1371/journal.pone.0075772.
30. Arap W, Pasqualini R, Ruoslahti E. Cancer treatment by targeted drug delivery to tumor vasculature in a mouse model. *Science (New York, N.Y.)*. 1998;279:377–380.
31. Arap W, Pasqualini R. The human vascular mapping project. Selection and utilization of molecules for tumor endothelial targeting. *Haemostasis*. 2001;31:30–31.
32. Staquicini FI, Cardo-Vila M, Kolonin MG, Trepel M, Edwards JK, Nunes DN, Sergeeva A, Efstathiou E, Sun J, Almeida NF, et al. Vascular ligand-receptor mapping by direct combinatorial selection in cancer patients. *Proc Natl Acad Sci USA*. 2011;108:18637–18642. DOI: 10.1073/pnas.1114503108.
33. Krag DN, Shukla GS, Shen GP, Pero S, Ashikaga T, Fuller S, Weaver DL, Burdette-Radoux S, Thomas C. Selection of tumor-binding ligands in cancer patients with phage display libraries. *Cancer Res*. 2006;66:7724–7733. DOI: 10.1158/0008-5472.CAN-05-4441.
34. Chung J, Shim H, Kim K, Lee D, Kim WJ, Kang DH, Kang SW, Jo H, Kwon K. Discovery of novel peptides targeting pro-atherogenic endothelium in disturbed flow regions -Targeted siRNA delivery to pro-atherogenic endothelium in vivo. *Sci Rep*. 2016;6:25636. DOI: 10.1038/srep25636.
35. Robert R, Jacobin-Valat MJ, Daret D, Miraux S, Nurden AT, Franconi JM, Clofent-Sanchez G. Identification of human scFvs targeting atherosclerotic lesions: selection by single round in vivo phage display. *J Biol Chem*. 2006;281:40135–40143. DOI: 10.1074/jbc.M609344200.
36. Deramchia K, Jacobin-Valat MJ, Vallet A, Bazin H, Santarelli X, Sanchez S, Dos Santos P, Franconi JM, Claverol S, Bonetto S, et al. In vivo phage display to identify new human antibody fragments homing to atherosclerotic endothelial and subendothelial tissues. *Am J Pathol*. 2012;180:2576–2589. DOI: 10.1016/j.ajpath.2012.02.013.
37. Nickel W. The mystery of nonclassical protein secretion. A current view on cargo proteins and potential export routes. *Eur J Biochem*. 2003;270:2109–2119. DOI: 10.1046/j.1432-1033.2003.03577.x.
38. Paclik D, Werner L, Guckelberger O, Wiedenmann B, Sturm A. Galectins distinctively regulate central monocyte and macrophage function. *Cell Immunol*. 2011;271:97–103. DOI: 10.1016/j.cellimm.2011.06.003.
39. Wang L, Guo XL. Molecular regulation of galectin-3 expression and therapeutic implication in cancer progression. *Biomed Pharmacother*. 2016;78:165–171. DOI: 10.1016/j.biopha.2016.01.014.
40. Menini S, Iacobini C, Blasetti Fantauzzi C, Pesce CM, Pugliese G. Role of galectin-3 in obesity and impaired glucose homeostasis. *Oxid Med Cell Longev*. 2016;2016:9618092. DOI: 10.1155/2016/9618092.
41. Venkatraman A, Hardas S, Patel N, Singh Bajaj N, Arora G, Arora P. Galectin-3: an emerging biomarker in stroke and cerebrovascular diseases. *Eur J Neurol*. 2018;25:238–246. DOI: 10.1111/ene.13496.
42. Fort-Gallifa I, Hernandez-Aguilera A, Garcia-Heredia A, Cabre N, Luciano-Mateo F, Simo JM, Martin-Paredero V, Camps J, Joven J. Galectin-3 in peripheral artery disease. Relationships with markers of oxidative stress and inflammation. *Int J Mol Sci*. 2017;18:973. DOI: 10.3390/ijms18050973.
43. Schattner M. Platelets and galectins. *Ann Transl Med*. 2014;2:85.
44. Ahmed H, AlSadek DM. Galectin-3 as a potential target to prevent cancer metastasis. *Clin Med Insights Oncol*. 2015;9:113–121.
45. Song L, Tang JW, Owusu L, Sun MZ, Wu J, Zhang J. Galectin-3 in cancer. *Clinica Chimica Acta*. 2014;431:185–191. DOI: 10.1016/j.cca.2014.01.019.
46. Eliaz I. The role of galectin-3 as a marker of cancer and inflammation in a stage IV ovarian cancer patient with underlying pro-inflammatory comorbidities. *Case reports in oncology*. 2013;6:343–349. DOI: 10.1159/000353574.
47. Ruvolo PP. Galectin 3 as a guardian of the tumor microenvironment. *Biochim Biophys Acta*. 1863;2016:427–437. DOI: 10.1016/j.bbamcr.2015.08.008.
48. Demotte N, Wieers G, Van Der Smissen P, Moser M, Schmidt C, Thielemans K, Squifflet JL, Weynand B, Carrasco J, Lurquin C, et al. A galectin-3 ligand corrects the impaired function of human CD4 and CD8 tumor-infiltrating lymphocytes and favors tumor rejection in mice. *Can Res*. 2010;70:7476–7488. DOI: 10.1158/0008-5472.CAN-10-0761.
49. Hogas S, Bilha SC, Branisteanu D, Hogas M, Gaipov A, Kanbay M, Covic A. Potential novel biomarkers of cardiovascular dysfunction and disease: cardiotrophin-1, adipokines and galectin-3. *Arch Med Sci*. 2017;13:897–913. DOI: 10.5114/aoms.2016.58664.
50. Madrigal-Matute J, Lindholt JS, Fernandez-Garcia CE, Benito-Martin A, Burillo E, Zalba G, Beloqui O, Llamas-Granda P, Ortiz A, Egido J, et al. Galectin-3, a biomarker linking oxidative stress and inflammation with the clinical outcomes of patients with atherothrombosis. *J Am Heart Assoc*. 2014;3. DOI: 10.1161/JAHA.114.000785.
51. He XW, Li WL, Li C, Liu P, Shen YG, Zhu M, Jin XP. Serum levels of galectin-1, galectin-3, and galectin-9 are associated with large artery atherosclerotic stroke. *Sci Rep*. 2017;7:40994. DOI: 10.1038/srep40994.
52. Zhu W, Sano H, Nagai R, Fukuhara K, Miyazaki A, Horiuchi S. The role of galectin-3 in endocytosis of advanced glycation end products and modified low density lipoproteins. *Biochem Biophys Res Commun*. 2001;280:1183–1188. DOI: 10.1006/bbrc.2001.4256.
53. Dong R, Zhang M, Hu Q, Zheng S, Soh A, Zheng Y, Yuan H. Galectin-3 as a novel biomarker for disease diagnosis and a target for therapy (review). *Int J Mol Med*. 2018;41:599–614.
54. MacKinnon AC, Liu X, Hadoke PW, Miller MR, Newby DE, Sethi T. Inhibition of galectin-3 reduces atherosclerosis in apolipoprotein E-deficient mice. *Glycobiology*. 2013;23:654–663. DOI: 10.1093/glycob/cwt006.
55. Nachtigal M, Ghaffar A, Mayer EP. Galectin-3 gene inactivation reduces atherosclerotic lesions and adventitial inflammation in ApoE-deficient mice. *Am J Pathol*. 2008;172:247–255. DOI: 10.2353/ajpath.2008.070348.
56. Kadoglou NP, Sfyroeras GS, Spathis A, Gkekas C, Gastounioti A, Mantas G, Nikita KS, Karakitsos P, Liapis CD. Galectin-3, carotid plaque vulnerability, and potential effects of statin therapy. *Eur J Vasc Endovasc Surg*. 2015;49:4–9. DOI: 10.1016/j.ejvs.2014.10.009.
57. Chen X, Lin J, Hu T, Ren Z, Li L, Hameed I, Zhang X, Men C, Guo Y, Xu D, et al. Galectin-3 exacerbates ox-LDL-mediated endothelial injury by inducing inflammation via integrin beta1-RhoA-JNK signaling activation. *J Cell Physiol*. 2019;234:10990–11000.
58. Di Gregoli K, Somerville M, Bianco R, Thomas AC, Frankow A, Newby AC, George SJ, Jackson CL, Johnson JL. Galectin-3 identifies a subset of macrophages with a potential beneficial role in atherosclerosis. *Arterioscler Thromb Vasc Biol*. 2020;40:1491–1509. DOI: 10.1161/ATVBAHA.120.314252.
59. Willemsen L, de Winther MP. Macrophage subsets in atherosclerosis as defined by single-cell technologies. *J Pathol*. 2020;250:705–714. DOI: 10.1002/path.5392.
60. Lin JD, Nishi H, Poles J, Niu X, McCauley C, Rahman K, Brown EJ, Yeung ST, Vozhilla N, Weinstock A, et al. Single-cell analysis of fate-mapped macrophages reveals heterogeneity, including stem-like properties, during atherosclerosis progression and regression. *JCI insight*. 2019;4. DOI: 10.1172/jci.insight.124574.
61. Cochain C, Vafadarnejad E, Arampatzi P, Pelisek J, Winkels H, Ley K, Wolf D, Saliba AE, Zernecke A. Single-cell RNA-Seq reveals the transcriptional landscape and heterogeneity of aortic macrophages in murine atherosclerosis. *Circ Res*. 2018;122:1661–1674. DOI: 10.1161/CIRCRESAHA.117.312509.
62. Kim K, Shim D, Lee JS, Zaitsev K, Williams JW, Kim KW, Jang MY, Seok Jang H, Yun TJ, Lee SH, et al. Transcriptome analysis reveals nonfoamy rather than foamy plaque macrophages are proinflammatory in atherosclerotic murine models. *Circ Res*. 2018;123:1127–1142. DOI: 10.1161/CIRCRESAHA.118.312804.
63. Inohara H, Akahani S, Koths K, Raz A. Interactions between galectin-3 and Mac-2-binding protein mediate cell-cell adhesion. *Cancer Res*. 1996;56:4530–4534.
64. Mondon P, Grand D, Souyris N, Emond S, Bouayadi K, Mutagen KH. A random mutagenesis method providing a complementary diversity generated by human error-prone DNA polymerases. *Methods Mol Biol (Clifton. NJ)*. 2010;634:373–386.

Downloaded from http://ahajournals.org by on October 1, 2021

SUPPLEMENTAL MATERIAL

Downloaded from http://ahajournals.org by on October 1, 2021

Table S1. LC/MS/MS analyses.

Accession	Description	MW [kDa]	Abundance Ratio: (Gal3Ab-Gal3R) / (P3-PH)	Abundance Ratio: (C4-PH) / (P3-PH)	Abundances: P3-PH	Abundances: Gal3Ab-Gal3R	Abundances: C4-PH
P04264	Keratin. type II cytoskeletal 1 OS=Homo sapiens OX=9606 GN=KRT1 PE=1 SV=6	66	2.33	1.225	45 381 190	105 509 281	55 462 114
P35527	Keratin. type I cytoskeletal 9 OS=Homo sapiens OX=9606 GN=KRT9 PE=1 SV=3	62	2.616	1.106	526 112 111	1 368 298 427	826 012 151
P13645	Keratin. type I cytoskeletal 10 OS=Homo sapiens OX=9606 GN=KRT10 PE=1 SV=6	58.8	1.188	1.332	807 546 518	923 347 631	1 097 290 637
P13647	Keratin. type II cytoskeletal 5 OS=Homo sapiens OX=9606 GN=KRT5 PE=1 SV=3	62.3	1.701	1.701	58 165 573	117 840 313	111 121 533
P15924	Desmoplakin OS=Homo sapiens OX=9606 GN=DSP PE=1 SV=3	331.6	2.345	1.134	22 454 072	52 833 781	23 573 337
P02538	Keratin. type II cytoskeletal 6A OS=Homo sapiens OX=9606 GN=KRT6A PE=1 SV=3	60	1.454	0.375	10 841 863	15 352 283	3 805 985
P04259	Keratin. type II cytoskeletal 6B OS=Homo sapiens OX=9606 GN=KRT6B PE=1 SV=5	60	0.859	0.588	5 179 109	4 525 792	2 750 493
P02533	Keratin. type I cytoskeletal 14 OS=Homo sapiens OX=9606 GN=KRT14 PE=1 SV=4	51.5	1.374	1.24	32 955 718	50 877 777	38 641 899
P08779	Keratin. type I cytoskeletal 16 OS=Homo sapiens OX=9606 GN=KRT16 PE=1 SV=4	51.2	1.266	0.551	28 412 636	35 940 365	15 478 307
P21333	Filamin-A OS=Homo sapiens OX=9606 GN=FLNA PE=1 SV=4	280.6	0.837	31.76	2 331 699	113 268	184 168 581
P78385	Keratin. type II cuticular Hb3 OS=Homo sapiens OX=9606 GN=KRT83 PE=1 SV=2	54.2	0.001	0.001	8 831 388		
Q86YZ3	Hornerin OS=Homo sapiens OX=9606 GN=HRNR PE=1 SV=2	282.2	3.61	1.218	3 849 321	12 238 252	4 518 731
P01857	Immunoglobulin heavy constant gamma 1 OS=Homo sapiens OX=9606 GN=IGHG1 PE=1 SV=1	36.1	0.787	166.4	10 092 989	8 868 397	1 783 465 295
P14923	Junction plakoglobin OS=Homo sapiens OX=9606 GN=JUP PE=1 SV=3	81.7	2.038	1.186	12 809 734	27 080 217	15 755 277
Q02413	Desmoglein-1 OS=Homo sapiens OX=9606 GN=DSG1 PE=1 SV=2	113.7	1.072	1.394	8 753 901	11 331 669	12 730 080

Downloaded from http://ahajournals.org by on October 1, 2021

Q04695	Keratin. type I cytoskeletal 17 OS=Homo sapiens OX=9606 GN=KRT17 PE=1 SV=2	48.1	4.332	1.145	2 988 213	14 015 720	3 406 516
P01834	Immunoglobulin kappa constant OS=Homo sapiens OX=9606 GN=IGKC PE=1 SV=2	11.8	0.392	124.2	7 322 950	3 760 060	1 031 345 071
Q7Z794	Keratin. type II cytoskeletal 1b OS=Homo sapiens OX=9606 GN=KRT77 PE=2 SV=3	61.9	0.808	0.813	46 801 707	107 950 795	77 872 103
P60709	Actin. cytoplasmic 1 OS=Homo sapiens OX=9606 GN=ACTB PE=1 SV=1	41.7	2.303	23.77	4 824 083	10 907 767	127 722 848
P62736	Actin. aortic smooth muscle OS=Homo sapiens OX=9606 GN=ACTA2 PE=1 SV=1	42	2.389	24.64	4 088 968	2 068 499	168 336 149
P07355	Annexin A2 OS=Homo sapiens OX=9606 GN=ANXA2 PE=1 SV=2	38.6	1.416	12.17	7 486 298	11 472 053	96 256 829
P35749	Myosin-11 OS=Homo sapiens OX=9606 GN=MYH11 PE=1 SV=3	227.2	0.757	13.97	125 171	226 226	22 645 844
P02751	Fibronectin OS=Homo sapiens OX=9606 GN=FN1 PE=1 SV=4	262.5	1.323	39.27	554 226	68 658	69 405 208
P12035	Keratin. type II cytoskeletal 3 OS=Homo sapiens OX=9606 GN=KRT3 PE=1 SV=3	64.4	1.684	1.922	160 742	602 931	683 572
P35579	Myosin-9 OS=Homo sapiens OX=9606 GN=MYH9 PE=1 SV=4	226.4	1000	1000		502 752	15 683 738
P04114	Apolipoprotein B-100 OS=Homo sapiens OX=9606 GN=APOB PE=1 SV=2	515.3	1000	1000		49 359	26 384 937
O95678	Keratin. type II cytoskeletal 75 OS=Homo sapiens OX=9606 GN=KRT75 PE=1 SV=2	59.5	0.001	0.001	459 243		
P01860	Immunoglobulin heavy constant gamma 3 OS=Homo sapiens OX=9606 GN=IGHG3 PE=1 SV=2	41.3		1000			39 436 191
Q8N1N4	Keratin. type II cytoskeletal 78 OS=Homo sapiens OX=9606 GN=KRT78 PE=1 SV=2	56.8	1.64	1.527	5 945 200	9 888 203	7 946 357
P01859	Immunoglobulin heavy constant gamma 2 OS=Homo sapiens OX=9606 GN=IGHG2 PE=1 SV=2	35.9	2.117	77.93	795 076	1 426 712	54 255 233
P35580	Myosin-10 OS=Homo sapiens OX=9606 GN=MYH10 PE=1 SV=3	228.9	0.001	3.44	147 192		10 681 021
P08670	Vimentin OS=Homo sapiens OX=9606 GN=VIM PE=1 SV=4	53.6	0.048	6.615	10 735 669	87 097	75 379 085

Downloaded from http://ahajournals.org by on October 1, 2021

P19013	Keratin. type II cytoskeletal 4 OS=Homo sapiens OX=9606 GN=KRT4 PE=1 SV=4	57.3	1.97	0.274	8 086 080	16 872 053	1 770 839
P13646	Keratin. type I cytoskeletal 13 OS=Homo sapiens OX=9606 GN=KRT13 PE=1 SV=4	49.6	2.499	0.765	2 982 381	7 565 975	1 542 532
P12111	Collagen alpha-3(VI) chain OS=Homo sapiens OX=9606 GN=COL6A3 PE=1 SV=5	343.5	0.524	17.83	648 511	79 816	47 866 537
Q92764	Keratin. type I cuticular Ha5 OS=Homo sapiens OX=9606 GN=KRT35 PE=2 SV=5	50.3	2.236	0.001	7 709 838	8 583 421	
Q05707	Collagen alpha-1(XIV) chain OS=Homo sapiens OX=9606 GN=COL14A1 PE=1 SV=3	193.4		79.17	31 329	78 467	41 524 411
Q9Y490	Talin-1 OS=Homo sapiens OX=9606 GN=TLN1 PE=1 SV=3	269.6		1000			16 445 393
P46940	Ras GTPase-activating-like protein IQGAP1 OS=Homo sapiens OX=9606 GN=IQGAP1 PE=1 SV=1	189.1	3.172	6.531	299 520	792 296	28 319 279
P04406	Glyceraldehyde-3-phosphate dehydrogenase OS=Homo sapiens OX=9606 GN=GAPDH PE=1 SV=3	36	1.366	3.607	3 766 910	6 067 009	18 817 508
Q5D862	Filaggrin-2 OS=Homo sapiens OX=9606 GN=FLG2 PE=1 SV=1	247.9	1.166	1.126	1 865 274	2 525 897	1 940 336
P29508	Serpin B3 OS=Homo sapiens OX=9606 GN=SERPINB3 PE=1 SV=2	44.5	4.519	1.273	2 665 624	15 747 547	3 565 204
P26038	Moesin OS=Homo sapiens OX=9606 GN=MSN PE=1 SV=3	67.8	1000	1000		28 527	14 284 505
A0A286YFJ8	Immunoglobulin heavy constant gamma 4 (Fragment) OS=Homo sapiens OX=9606 GN=IGHG4 PE=1 SV=1	43.8	1000	1000		32 076	6 207 931
P05089	Arginase-1 OS=Homo sapiens OX=9606 GN=ARG1 PE=1 SV=2	34.7	1.338	1.118	2 450 206	2 929 382	2 874 411
Q08554	Desmocollin-1 OS=Homo sapiens OX=9606 GN=DSC1 PE=1 SV=2	99.9	1.212	2.119	3 353 097	4 710 847	7 365 633
Q5T749	Keratinocyte proline-rich protein OS=Homo sapiens OX=9606 GN=KPRP PE=1 SV=1	64.1	1.095	1.608	4 589 295	7 546 455	10 630 003
P17931	Galectin-3 OS=Homo sapiens OX=9606 GN=LGALS3 PE=1 SV=5	26.1	0.739	0.037	35 326 405	30 552 241	1 266 731

Downloaded from http://ahajournals.org by on October 1, 2021

E9PKE3	Heat shock cognate 71 kDa protein OS=Homo sapiens OX=9606 GN=HSPA8 PE=1 SV=1	68.8	1000	1000		535 457	2 435 736
Q08188	Protein-glutamine gamma-glutamyltransferase E OS=Homo sapiens OX=9606 GN=TGM3 PE=1 SV=4	76.6	1.256	0.907	4 132 727	5 165 512	3 745 956
P04083	Annexin A1 OS=Homo sapiens OX=9606 GN=ANXA1 PE=1 SV=2	38.7	1.51	2.346	3 110 045	4 500 463	8 648 641
P12814	Alpha-actinin-1 OS=Homo sapiens OX=9606 GN=ACTN1 PE=1 SV=2	103	0.001	18.98	54 288		2 606 953
Q7Z3Y8	Keratin. type I cytoskeletal 27 OS=Homo sapiens OX=9606 GN=KRT27 PE=1 SV=2	49.8	0.001	2.116	690 173		1 986 529
Q13813	Spectrin alpha chain. non-erythrocytic 1 OS=Homo sapiens OX=9606 GN=SPTAN1 PE=1 SV=3	284.4	0.592	3.895	32 298	68 760	5 824 759
P01024	Complement C3 OS=Homo sapiens OX=9606 GN=C3 PE=1 SV=2	187	1.11	14.65	238 945	658 899	9 816 719
Q3SY84	Keratin. type II cytoskeletal 71 OS=Homo sapiens OX=9606 GN=KRT71 PE=1 SV=3	57.3	0.001	2.108	1 631 769		1 702 343
P31944	Caspase-14 OS=Homo sapiens OX=9606 GN=CASP14 PE=1 SV=2	27.7	2.237	1.565	1 508 967	3 673 264	2 994 961
P02675	Fibrinogen beta chain OS=Homo sapiens OX=9606 GN=FGB PE=1 SV=2	55.9	1.682	21.6	204 267	81 373	14 895 512
P11021	Endoplasmic reticulum chaperone BiP OS=Homo sapiens OX=9606 GN=HSPA5 PE=1 SV=2	72.3	2.581	5.152	372 169	1 822 958	4 027 552
O43707	Alpha-actinin-4 OS=Homo sapiens OX=9606 GN=ACTN4 PE=1 SV=2	104.8	2.448	5.214	74 939	281 232	2 933 348
P25311	Zinc-alpha-2-glycoprotein OS=Homo sapiens OX=9606 GN=AZGP1 PE=1 SV=2	34.2	0.618	1.454	4 171 075	2 627 848	6 422 387
P0DOY3	Immunoglobulin lambda constant 3 OS=Homo sapiens OX=9606 GN=IGLC3 PE=1 SV=1	11.3	1000	1000		63 879	23 435 315
P06702	Protein S100-A9 OS=Homo sapiens OX=9606 GN=S100A9 PE=1 SV=1	13.2	2.549	1.011	3 260 708	9 956 036	4 538 845
Q71U36	Tubulin alpha-1A chain OS=Homo sapiens OX=9606 GN=TUBA1A PE=1 SV=1	50.1	2.052	27.53	362 570	745 243	10 901 197

Downloaded from http://ahajournals.org by on October 1, 2021

P02649	Apolipoprotein E OS=Homo sapiens OX=9606 GN=APOE PE=1 SV=1	36.1	0.001	24.7	889 811		40 309 038
Q6KB66	Keratin. type II cytoskeletal 80 OS=Homo sapiens OX=9606 GN=KRT80 PE=1 SV=2	50.5	1.725	1.046	2 250 313	4 044 348	2 511 371
Q15063	Periostin OS=Homo sapiens OX=9606 GN=POSTN PE=1 SV=2	93.3	0.001	70.78	35 600		13 290 139
A0A1B0GUU9	Immunoglobulin heavy constant mu (Fragment) OS=Homo sapiens OX=9606 GN=IGHM PE=1 SV=1	51.9	0.171	11.48	2 232 212	92 462	26 343 097
P55072	Transitional endoplasmic reticulum ATPase OS=Homo sapiens OX=9606 GN=VCP PE=1 SV=4	89.3	0.123	0.099	8 671 478	1 549 892	2 472 195
Q14CN4	Keratin. type II cytoskeletal 72 OS=Homo sapiens OX=9606 GN=KRT72 PE=1 SV=2	55.8	0.438		1 825 028	1 574 891	34 582
A0A087WVV2	Ribosome-binding protein 1 OS=Homo sapiens OX=9606 GN=RRBP1 PE=1 SV=1	102.7		1000			3 987 261
P04004	Vitronectin OS=Homo sapiens OX=9606 GN=VTN PE=1 SV=1	54.3	0.638	85.16	810 878	160 756	71 415 327
Q8IUX7	Adipocyte enhancer-binding protein 1 OS=Homo sapiens OX=9606 GN=AEBP1 PE=1 SV=1	130.8		1000			11 142 930
P68371	Tubulin beta-4B chain OS=Homo sapiens OX=9606 GN=TUBB4B PE=1 SV=1	49.8	5.825	14.72	19 223	152 610	1 062 723
Q6UWP8	Suprabasin OS=Homo sapiens OX=9606 GN=SBSN PE=1 SV=2	60.5	1.615	1.485	246 320	583 046	320 064
A0A0B4J231	Immunoglobulin lambda-like polypeptide 5 OS=Homo sapiens OX=9606 GN=IGLL5 PE=1 SV=1	23.1	2.034	121.9	133 573	271 643	23 571 627
A0A087X0S5	Collagen alpha-1(VI) chain OS=Homo sapiens OX=9606 GN=COL6A1 PE=1 SV=1	108.3	0.001	66.33	242 097		30 154 159
Q09666	Neuroblast differentiation-associated protein AHNAK OS=Homo sapiens OX=9606 GN=AHNAK PE=1 SV=2	628.7	0.761	7.562	469 657	286 623	4 292 521
Q13867	Bleomycin hydrolase OS=Homo sapiens OX=9606 GN=BLMH PE=1 SV=1	52.5	1.957	1.198	1 304 594	2 335 275	1 614 657

Downloaded from http://ahajournals.org by on October 1, 2021

Q99715	Collagen alpha-1(XII) chain OS=Homo sapiens OX=9606 GN=COL12A1 PE=1 SV=2	332.9	0.001	5.481	25 882		4 187 082
P02545	Prelamin-A/C OS=Homo sapiens OX=9606 GN=LMNA PE=1 SV=1	74.1	3.833	10.01	572 827	2 978 452	5 817 524
P21810	Biglycan OS=Homo sapiens OX=9606 GN=BGN PE=1 SV=2	41.6	0.001	93.09	164 572		50 722 913
P02647	Apolipoprotein A-I OS=Homo sapiens OX=9606 GN=APOA1 PE=1 SV=1	30.8	0.752	8.986	1 093 580	1 009 112	11 281 958
A0A0G2JIW1	Heat shock 70 kDa protein 1B OS=Homo sapiens OX=9606 GN=HSPA1B PE=1 SV=1	70.1	1.364	8.382	84 517	481 548	2 397 252
P51888	Prolargin OS=Homo sapiens OX=9606 GN=PRELP PE=1 SV=1	43.8	0.001	30.13	219 197		20 257 631
P15311	Ezrin OS=Homo sapiens OX=9606 GN=EZR PE=1 SV=4	69.4	1000	1000		41 623	436 838
A0A2R8Y5S7	Radixin OS=Homo sapiens OX=9606 GN=RDX PE=1 SV=1	69.3		1000			549 735
Q5JP53	Tubulin beta chain OS=Homo sapiens OX=9606 GN=TUBB PE=1 SV=1	47.7	0.94	53.18	22 422	21 076	5 706 720
C9JEU5	Fibrinogen gamma chain OS=Homo sapiens OX=9606 GN=FGG PE=1 SV=1	50.3	0.001	25.87	122 868		14 365 894
P10909	Clusterin OS=Homo sapiens OX=9606 GN=CLU PE=1 SV=1	52.5	0.348	40.32	361 040	95 260	22 649 197
J3QSU6	Tenascin OS=Homo sapiens OX=9606 GN=TNC PE=1 SV=1	220.7		1000			6 574 638
Q01082	Spectrin beta chain. non-erythrocytic 1 OS=Homo sapiens OX=9606 GN=SPTBN1 PE=1 SV=2	274.4		1000			2 599 602
P01876	Immunoglobulin heavy constant alpha 1 OS=Homo sapiens OX=9606 GN=IGHA1 PE=1 SV=2	37.6	0.713	3.226	3 276 026	2 484 800	12 871 867
P14618	Pyruvate kinase PKM OS=Homo sapiens OX=9606 GN=PKM PE=1 SV=4	57.9	2.228	7.358	645 019	1 894 485	6 566 692
P68104	Elongation factor 1-alpha 1 OS=Homo sapiens OX=9606 GN=EEF1A1 PE=1 SV=1	50.1	3.596	7.059	1 380 167	6 111 838	12 840 624

Downloaded from http://ahajournals.org by on October 1, 2021

P22735	Protein-glutamine gamma-glutamyltransferase K OS=Homo sapiens OX=9606 GN=TGM1 PE=1 SV=4	89.7	1.205	1.033	791 100	1 005 590	818 794
Q13835	Plakophilin-1 OS=Homo sapiens OX=9606 GN=PKP1 PE=1 SV=2	82.8	3.662	1.336	943 686	3 864 503	1 185 744
P04792	Heat shock protein beta-1 OS=Homo sapiens OX=9606 GN=HSPB1 PE=1 SV=2	22.8	3.509	11.81	785 763	3 944 150	18 569 316
P20930	Filaggrin OS=Homo sapiens OX=9606 GN=FLG PE=1 SV=3	434.9	2.074	1.084	612 555	1 573 109	816 305
P23284	Peptidyl-prolyl cis-trans isomerase B OS=Homo sapiens OX=9606 GN=PPIB PE=1 SV=2	23.7	1.016	24.38	59 248	112 122	62 051 286
A0A0C4DGN4	Zymogen granule protein 16 homolog B OS=Homo sapiens OX=9606 GN=ZG16B PE=1 SV=1	19.6	4.517	2.153	1 827 338	8 034 713	3 421 855
P06733	Alpha-enolase OS=Homo sapiens OX=9606 GN=ENO1 PE=1 SV=2	47.1	4.655	3.312	921 269	4 564 445	2 969 887
P98160	Basement membrane-specific heparan sulfate proteoglycan core protein OS=Homo sapiens OX=9606 GN=HSPG2 PE=1 SV=4	468.5		1000			1 922 225
P00734	Prothrombin OS=Homo sapiens OX=9606 GN=F2 PE=1 SV=2	70	1000	1000		68 460	6 723 894
P62805	Histone H4 OS=Homo sapiens OX=9606 GN=HIST1H4A PE=1 SV=2	11.4	4.228	0.481	2 814 698	16 733 421	1 202 205
P04196	Histidine-rich glycoprotein OS=Homo sapiens OX=9606 GN=HRG PE=1 SV=1	59.5		57.81	15 439	99 841	11 061 712
C9J406	MICOS complex subunit MIC60 OS=Homo sapiens OX=9606 GN=IMMT PE=1 SV=1	73.2		1000			4 407 636
P35442	Thrombospondin-2 OS=Homo sapiens OX=9606 GN=THBS2 PE=1 SV=2	129.9		1000			3 436 183
P01023	Alpha-2-macroglobulin OS=Homo sapiens OX=9606 GN=A2M PE=1 SV=3	163.2		7.245	170 500	43 721	3 469 375
Q08431	Lactadherin OS=Homo sapiens OX=9606 GN=MFGE8 PE=1 SV=3	43.1	0.001	27.93	154 872		19 943 799
E9PF17	Versican core protein OS=Homo sapiens OX=9606 GN=VCAN PE=1 SV=2	176.7	0.712	0.465	4 688 793	3 339 429	2 629 844

Downloaded from http://ahajournals.org by on October 1, 2021

Q01469	Fatty acid-binding protein 5 OS=Homo sapiens OX=9606 GN=FABP5 PE=1 SV=3	15.2	2.276	1.236	1 063 748	2 030 889	1 052 884
P31947	14-3-3 protein sigma OS=Homo sapiens OX=9606 GN=SFN PE=1 SV=1	27.8	5.962	0.001	194 048	2 695 048	
Q5QNW6	Histone H2B type 2-F OS=Homo sapiens OX=9606 GN=HIST2H2BF PE=1 SV=3	13.9	5.335	1.15	1 374 217	8 101 146	1 992 132
P05109	Protein S100-A8 OS=Homo sapiens OX=9606 GN=S100A8 PE=1 SV=1	10.8	2.245	1.816	3 413 420	8 180 162	6 171 888
P32119	Peroxiredoxin-2 OS=Homo sapiens OX=9606 GN=PRDX2 PE=1 SV=5	21.9	2.373	1.736	475 631	840 660	803 651
P12273	Prolactin-inducible protein OS=Homo sapiens OX=9606 GN=PIP PE=1 SV=1	16.6	0.487	1.866	1 561 619	693 561	3 541 678
Q96P63	Serpin B12 OS=Homo sapiens OX=9606 GN=SERPINB12 PE=1 SV=1	46.2	1.144	1.483	2 160 855	2 699 507	3 658 133
P00338	L-lactate dehydrogenase A chain OS=Homo sapiens OX=9606 GN=LDHA PE=1 SV=2	36.7	2.311	6.299	637 766	2 201 239	6 423 825
Q5JXI8	Four and a half LIM domains protein 1 (Fragment) OS=Homo sapiens OX=9606 GN=FHL1 PE=1 SV=1	29.1	0.001	42.77	283 968		44 626 126
P02671	Fibrinogen alpha chain OS=Homo sapiens OX=9606 GN=FGA PE=1 SV=2	94.9	0.001	13.01	242 044		9 308 706
Q6NZI2	Caveolae-associated protein 1 OS=Homo sapiens OX=9606 GN=CAVIN1 PE=1 SV=1	43.5		1000			8 956 870
P81605	Dermcidin OS=Homo sapiens OX=9606 GN=DCD PE=1 SV=2	11.3	0.878	1.349	1 597 868	1 409 168	2 108 953
P07996	Thrombospondin-1 OS=Homo sapiens OX=9606 GN=THBS1 PE=1 SV=2	129.3		1000			4 314 638
P07900	Heat shock protein HSP 90-alpha OS=Homo sapiens OX=9606 GN=HSP90AA1 PE=1 SV=5	84.6	1000	1000		224 887	2 127 037
Q8WWA0	Intelectin-1 OS=Homo sapiens OX=9606 GN=ITLN1 PE=1 SV=1	34.9	0.014	0.001	12 452 942	24 658	
P06576	ATP synthase subunit beta mitochondrial OS=Homo sapiens OX=9606 GN=ATP5F1B PE=1 SV=3	56.5	1.736	3.654	348 341	927 933	2 719 680
P01042	Kininogen-1 OS=Homo sapiens OX=9606 GN=KNG1 PE=1 SV=2	71.9	0.204	58.59	148 106	14 553	14 828 856

Downloaded from http://ahajournals.org by on October 1, 2021

P18206	Vinculin OS=Homo sapiens OX=9606 GN=VCL PE=1 SV=4	123.7	0.682	6.079	209 980	80 825	2 489 326
P60174	Triosephosphate isomerase OS=Homo sapiens OX=9606 GN=TPI1 PE=1 SV=3	30.8	2.343	0.92	275 550	779 269	347 355
B7Z6Z4	cDNA FLJ56329. highly similar to Myosin light polypeptide 6 OS=Homo sapiens OX=9606 GN=MYL6 PE=1 SV=1	26.7	1000	1000		151 145	8 869 697
J3QR68	Haptoglobin (Fragment) OS=Homo sapiens OX=9606 GN=HP PE=1 SV=1	45	0.923	3.686	296 485	214 197	1 595 809
P12110	Collagen alpha-2(VI) chain OS=Homo sapiens OX=9606 GN=COL6A2 PE=1 SV=4	108.5	1.22	31.02	303 644	132 739	13 859 775
P51884	Lumican OS=Homo sapiens OX=9606 GN=LUM PE=1 SV=2	38.4	0.001	13.52	556 747		9 128 102
P21291	Cysteine and glycine-rich protein 1 OS=Homo sapiens OX=9606 GN=CSRP1 PE=1 SV=3	20.6	0.001	17.55	284 626		15 167 061
P08133	Annexin A6 OS=Homo sapiens OX=9606 GN=ANXA6 PE=1 SV=3	75.8	0.001	7.254	59 216		2 881 655
P08238	Heat shock protein HSP 90-beta OS=Homo sapiens OX=9606 GN=HSP90AB1 PE=1 SV=4	83.2	1000	1000		116 746	1 181 134
O75342	Arachidonate 12-lipoxygenase. 12R-type OS=Homo sapiens OX=9606 GN=ALOX12B PE=1 SV=1	80.3	1.134	1.661	290 418	312 236	519 182
Q16527	Cysteine and glycine-rich protein 2 OS=Homo sapiens OX=9606 GN=CSRP2 PE=1 SV=3	20.9		1000			8 578 199
Q01995	Transgelin OS=Homo sapiens OX=9606 GN=TAGLN PE=1 SV=4	22.6	0.001	2.437	1 301 022		3 375 481
Q14574	Desmocollin-3 OS=Homo sapiens OX=9606 GN=DSC3 PE=1 SV=3	99.9	1.207	1.717	536 353	725 441	930 781
P14625	Endoplasmin OS=Homo sapiens OX=9606 GN=HSP90B1 PE=1 SV=1	92.4		1000			3 495 217
P00747	Plasminogen OS=Homo sapiens OX=9606 GN=PLG PE=1 SV=2	90.5		1000			2 546 712
P02743	Serum amyloid P-component OS=Homo sapiens OX=9606 GN=APCS PE=1 SV=2	25.4	0.001	40.22	1 163 541		63 837 550
P31151	Protein S100-A7 OS=Homo sapiens OX=9606 GN=S100A7 PE=1 SV=4	11.5	1.801	1.167	434 969	1 507 674	420 937

Downloaded from http://ahajournals.org by on October 1, 2021

A0A0A0MSV6	Complement C1q subcomponent subunit B (Fragment) OS=Homo sapiens OX=9606 GN=C1QB PE=1 SV=6	24	0.001	9.824	428 154		8 474 815
Q15582	Transforming growth factor-beta-induced protein ig-h3 OS=Homo sapiens OX=9606 GN=TGFBI PE=1 SV=1	74.6		1000			2 506 857
P02748	Complement component C9 OS=Homo sapiens OX=9606 GN=C9 PE=1 SV=2	63.1	0.001	7.126	504 499		4 953 838
P01040	Cystatin-A OS=Homo sapiens OX=9606 GN=CSTA PE=1 SV=1	11	0.456	2.506	2 057 646	996 644	4 641 774
Q6ZN40	Tropomyosin 1 (Alpha). isoform CRA_f OS=Homo sapiens OX=9606 GN=TPM1 PE=1 SV=1	37.4	0.001	2.366	68 650		1 172 949
M0QZK8	Uncharacterized protein OS=Homo sapiens OX=9606 PE=4 SV=1	11.6	1.305	1.083	735 058	1 416 610	789 921
P50995	Annexin A11 OS=Homo sapiens OX=9606 GN=ANXA11 PE=1 SV=1	54.4	0.836	23.31	47 232	39 505	3 238 475
Q15149	Plectin OS=Homo sapiens OX=9606 GN=PLEC PE=1 SV=3	531.5		1000			831 389
P01009	Alpha-1-antitrypsin OS=Homo sapiens OX=9606 GN=SERPINA1 PE=1 SV=3	46.7	0.523	4.59	487 599	194 996	3 303 390
P51911	Calponin-1 OS=Homo sapiens OX=9606 GN=CNN1 PE=1 SV=2	33.2	0.001	10.09	165 932		4 661 641
Q16270	Insulin-like growth factor-binding protein 7 OS=Homo sapiens OX=9606 GN=IGFBP7 PE=1 SV=1	29.1		1000			3 480 607
P19823	Inter-alpha-trypsin inhibitor heavy chain H2 OS=Homo sapiens OX=9606 GN=ITIH2 PE=1 SV=2	106.4		1000			2 145 534
G8JLG2	CDSN OS=Homo sapiens OX=9606 GN=CDSN PE=1 SV=1	51.6	1.406	2.676	601 717	859 709	1 593 342
Q16853	Membrane primary amine oxidase OS=Homo sapiens OX=9606 GN=AOC3 PE=1 SV=3	84.6	1.142	12.45	101 673	50 740	7 642 017
P40926	Malate dehydrogenase mitochondrial OS=Homo sapiens OX=9606 GN=MDH2 PE=1 SV=3	35.5	4.425	0.952	52 219	1 304 570	256 434

Downloaded from http://ahajournals.org by on October 1, 2021

E9PFZ2	Ceruloplasmin OS=Homo sapiens OX=9606 GN=CP PE=1 SV=1	108.8	2.636	4.613	51 090	230 909	461 703
Q9NZT1	Calmodulin-like protein 5 OS=Homo sapiens OX=9606 GN=CALML5 PE=1 SV=2	15.9	4.925	1.261	397 533	3 028 257	501 469
P00558	Phosphoglycerate kinase 1 OS=Homo sapiens OX=9606 GN=PGK1 PE=1 SV=3	44.6	0.99	6.25	64 337	145 614	1 043 848
P02792	Ferritin light chain OS=Homo sapiens OX=9606 GN=FTL PE=1 SV=2	20	0.001	4.161	834 926		3 631 057
P07384	Calpain-1 catalytic subunit OS=Homo sapiens OX=9606 GN=CAPN1 PE=1 SV=1	81.8	1.426	4.129	174 509	409 520	2 052 887
P02747	Complement C1q subcomponent subunit C OS=Homo sapiens OX=9606 GN=C1QC PE=1 SV=3	25.8	0.001	9.491	405 030		8 785 534
P61160	Actin-related protein 2 OS=Homo sapiens OX=9606 GN=ACTR2 PE=1 SV=1	44.7	1000	1000		59 391	1 738 341
P07476	Involucrin OS=Homo sapiens OX=9606 GN=IVL PE=1 SV=2	68.4	1000			831 200	
A0A087WVQ6	Clathrin heavy chain OS=Homo sapiens OX=9606 GN=CLTC PE=1 SV=1	191.9	1000	1000		52 669	933 697
F5GXS0	Complement C4-B OS=Homo sapiens OX=9606 GN=C4B PE=1 SV=1	187.6	0.001	17.49	38 162		1 269 947
H0Y7A7	Calmodulin-2 (Fragment) OS=Homo sapiens OX=9606 GN=CALM2 PE=1 SV=1	20.7	1000	1000		1 269 146	51 075
P07237	Protein disulfide-isomerase OS=Homo sapiens OX=9606 GN=P4HB PE=1 SV=3	57.1	3.062	8.215	28 459	163 283	1 129 350
Q16610	Extracellular matrix protein 1 OS=Homo sapiens OX=9606 GN=ECM1 PE=1 SV=2	60.6	2.306	1.33	126 503	365 994	214 816
P08603	Complement factor H OS=Homo sapiens OX=9606 GN=CFH PE=1 SV=4	139		1000			788 827
P46821	Microtubule-associated protein 1B OS=Homo sapiens OX=9606 GN=MAP1B PE=1 SV=2	270.5		1000			2 261 574
P52943	Cysteine-rich protein 2 OS=Homo sapiens OX=9606 GN=CRIP2 PE=1 SV=1	22.5		1000			6 350 152
Q5T750	Skin-specific protein 32 OS=Homo sapiens OX=9606 GN=XP32 PE=1 SV=1	26.2	1.082	1.131	2 618 564	3 416 486	2 974 391

Downloaded from http://ahajournals.org by on October 1, 2021

P30101	Protein disulfide-isomerase A3 OS=Homo sapiens OX=9606 GN=PDIA3 PE=1 SV=4	56.7	1000	1000		64 313	1 374 169
Q9NZU5	LIM and cysteine-rich domains protein 1 OS=Homo sapiens OX=9606 GN=LMCD1 PE=1 SV=1	40.8		1000			1 172 181
P04003	C4b-binding protein alpha chain OS=Homo sapiens OX=9606 GN=C4BPA PE=1 SV=2	67	0.001	20.91	41 215		4 607 305
P00491	Purine nucleoside phosphorylase OS=Homo sapiens OX=9606 GN=PNP PE=1 SV=2	32.1	2.457	1.41	89 423	346 441	126 090
A0A0A0MTH3	Integrin-linked protein kinase OS=Homo sapiens OX=9606 GN=ILK PE=1 SV=1	54.6		1000			721 621
P09382	Galectin-1 OS=Homo sapiens OX=9606 GN=LGALS1 PE=1 SV=2	14.7		1000			1 819 743
P30837	Aldehyde dehydrogenase X. mitochondrial OS=Homo sapiens OX=9606 GN=ALDH1B1 PE=1 SV=3	57.2		1000			420 189
C9JF17	Apolipoprotein D (Fragment) OS=Homo sapiens OX=9606 GN=APOD PE=1 SV=1	24.1	0.21	3.809	827 521	48 247	2 980 241
X6RJP6	Transgelin-2 (Fragment) OS=Homo sapiens OX=9606 GN=TAGLN2 PE=1 SV=1	21.1		8.921	51 188	53 473	2 778 755
P01833	Polymeric immunoglobulin receptor OS=Homo sapiens OX=9606 GN=PIGR PE=1 SV=4	83.2	1.263	1.477	1 054 297	1 054 565	1 240 193
G3V3U4	Proteasome subunit alpha type OS=Homo sapiens OX=9606 GN=PSMA6 PE=1 SV=1	11.6	1.361	1.508	345 184	439 769	548 912
P09525	Annexin A4 OS=Homo sapiens OX=9606 GN=ANXA4 PE=1 SV=4	35.9	1000	1000		371 153	418 889
P0DPA2	V-set and immunoglobulin domain-containing protein 8 OS=Homo sapiens OX=9606 GN=VSIG8 PE=2 SV=1	43.9	0.062	0.001	1 071 003	44 472	
Q08380	Galectin-3-binding protein OS=Homo sapiens OX=9606 GN=LGALS3BP PE=1 SV=1	65.3	0.001	11.32	40 712		1 175 630
P17655	Calpain-2 catalytic subunit OS=Homo sapiens OX=9606 GN=CAPN2 PE=1 SV=6	79.9		1000			1 258 940
P48745	CCN family member 3 OS=Homo sapiens OX=9606 GN=CCN3 PE=1 SV=1	39.1		1000			1 585 307

Downloaded from http://ahajournals.org by on October 1, 2021

P03950	Angiogenin OS=Homo sapiens OX=9606 GN=ANG PE=1 SV=1	16.5		1000			7 008 451
B7ZKJ8	ITIH4 protein OS=Homo sapiens OX=9606 GN=ITIH4 PE=1 SV=1	103.8		13.54	27 611	28 165	1 166 765
O14818	Proteasome subunit alpha type-7 OS=Homo sapiens OX=9606 GN=PSMA7 PE=1 SV=1	27.9	1.39	1.49	166 918	331 016	456 350
A0A0C4DH38	Immunoglobulin heavy variable 5-51 OS=Homo sapiens OX=9606 GN=IGHV5-51 PE=3 SV=1	12.7		1000			3 613 847
P01011	Alpha-1-antichymotrypsin OS=Homo sapiens OX=9606 GN=SERPINA3 PE=1 SV=2	47.6	0.792	2.341	524 467	339 828	1 961 292
P07737	Profilin-1 OS=Homo sapiens OX=9606 GN=PFN1 PE=1 SV=2	15	2.002	10.76	73 160	200 657	1 187 235
E9PK25	Cofilin-1 OS=Homo sapiens OX=9606 GN=CFL1 PE=1 SV=1	22.7	3.301	18.5	73 612	291 701	1 902 475
P06727	Apolipoprotein A-IV OS=Homo sapiens OX=9606 GN=APOA4 PE=1 SV=3	45.4		1000			1 254 604
Q15046	Lysine--tRNA ligase OS=Homo sapiens OX=9606 GN=KARS PE=1 SV=3	68		1000			728 628
P00325	Alcohol dehydrogenase 1B OS=Homo sapiens OX=9606 GN=ADH1B PE=1 SV=2	39.8	0.001	8.389	92 282		1 151 690
K7EK77	ATP synthase subunit alpha mitochondrial (Fragment) OS=Homo sapiens OX=9606 GN=ATP5F1A PE=1 SV=1	22.2	1.867	7.849	95 222	253 308	1 919 224
Q9UI42	Carboxypeptidase A4 OS=Homo sapiens OX=9606 GN=CPA4 PE=1 SV=2	47.3	1.011	1.191	436 078	489 788	518 292
Q9NR12	PDZ and LIM domain protein 7 OS=Homo sapiens OX=9606 GN=PDLIM7 PE=1 SV=1	49.8		1000			2 352 668
P21980	Protein-glutamine gamma-glutamyltransferase 2 OS=Homo sapiens OX=9606 GN=TGM2 PE=1 SV=2	77.3		1000			599 576
P59998	Actin-related protein 2/3 complex subunit 4 OS=Homo sapiens OX=9606 GN=ARPC4 PE=1 SV=3	19.7	1.714	23.86	72 430	229 689	3 163 160
A0A0A0MSQ0	Plastin-3 OS=Homo sapiens OX=9606 GN=PLS3 PE=1 SV=1	69.3	1000	1000		44 104	78 282

Downloaded from http://ahajournals.org by on October 1, 2021

J3KNQ4	Alpha-parvin OS=Homo sapiens OX=9606 GN=PARVA PE=1 SV=1	46.6		1000			226 091
P47929	Galectin-7 OS=Homo sapiens OX=9606 GN=LGALS7 PE=1 SV=2	15.1	10.594	0.829	656 160	6 022 365	568 841
P29536	Leiomodin-1 OS=Homo sapiens OX=9606 GN=LMOD1 PE=1 SV=3	67		1000			3 109 431
P20774	Mimecan OS=Homo sapiens OX=9606 GN=OGN PE=1 SV=1	33.9	0.001	15.44	469 785		6 874 894
Q8WX93	Palladin OS=Homo sapiens OX=9606 GN=PALLD PE=1 SV=3	150.5		1000			716 729
Q9H3U7	SPARC-related modular calcium-binding protein 2 OS=Homo sapiens OX=9606 GN=SMOC2 PE=2 SV=2	49.6		1000			646 965
P48735	Isocitrate dehydrogenase [NADP] mitochondrial OS=Homo sapiens OX=9606 GN=IDH2 PE=1 SV=2	50.9		1000			410 840
P10301	Ras-related protein R-Ras OS=Homo sapiens OX=9606 GN=RRAS PE=1 SV=1	23.5		1000			625 649
P08294	Extracellular superoxide dismutase [Cu-Zn] OS=Homo sapiens OX=9606 GN=SOD3 PE=1 SV=2	25.8		1000			2 150 059
P62140	Serine/threonine-protein phosphatase PP1-beta catalytic subunit OS=Homo sapiens OX=9606 GN=PPP1CB PE=1 SV=3	37.2		1000			346 858
P18669	Phosphoglycerate mutase 1 OS=Homo sapiens OX=9606 GN=PGAM1 PE=1 SV=2	28.8	1000	1000		168 058	415 579
Q96QA5	Gasdermin-A OS=Homo sapiens OX=9606 GN=GSDMA PE=1 SV=4	49.3	1.357	1.406	660 379	879 530	912 017
Q07960	Rho GTPase-activating protein 1 OS=Homo sapiens OX=9606 GN=ARHGAP1 PE=1 SV=1	50.4		1000			671 085
A0A3B3IRN5	Fibromodulin OS=Homo sapiens OX=9606 GN=FMOD PE=1 SV=1	32.7	0.001	11.33	75 912		1 829 809
P07225	Vitamin K-dependent protein S OS=Homo sapiens OX=9606 GN=PROS1 PE=1 SV=1	75.1		1000			2 039 996
E9PHK0	Tetranectin OS=Homo sapiens OX=9606 GN=CLEC3B PE=1 SV=1	17.8		1000			822 733

Downloaded from http://ahajournals.org by on October 1, 2021

P06312	Immunoglobulin kappa variable 4-1 OS=Homo sapiens OX=9606 GN=IGKV4-1 PE=1 SV=1	13.4		1000			13 190 201
P13796	Plastin-2 OS=Homo sapiens OX=9606 GN=LCP1 PE=1 SV=6	70.2		1000			307 084
E9PK52	Band 4.1-like protein 2 OS=Homo sapiens OX=9606 GN=EPB41L2 PE=1 SV=1	90.9		1000			374 576
Q03135	Caveolin-1 OS=Homo sapiens OX=9606 GN=CAV1 PE=1 SV=4	20.5		1000			4 081 415
Q9ULV4	Coronin-1C OS=Homo sapiens OX=9606 GN=CORO1C PE=1 SV=1	53.2		1000			907 308
Q9HC84	Mucin-5B OS=Homo sapiens OX=9606 GN=MUC5B PE=1 SV=3	596	0.925	0.001	119 972	110 987	
B7Z4L4	Dolichyl-diphosphooligosaccharide--protein glycosyltransferase subunit 1 OS=Homo sapiens OX=9606 GN=RPN1 PE=1 SV=1	49.9	2.441	15.9	19 587	47 819	605 229
P20851	C4b-binding protein beta chain OS=Homo sapiens OX=9606 GN=C4BPB PE=1 SV=1	28.3		1000			1 331 937
P27824	Calnexin OS=Homo sapiens OX=9606 GN=CANX PE=1 SV=2	67.5		1000			1 905 619
P00740	Coagulation factor IX OS=Homo sapiens OX=9606 GN=F9 PE=1 SV=2	51.7		1000			1 897 252
P05164	Myeloperoxidase OS=Homo sapiens OX=9606 GN=MPO PE=1 SV=1	83.8	1.143	1.747	154 701	368 143	358 838
Q96CG8	Collagen triple helix repeat-containing protein 1 OS=Homo sapiens OX=9606 GN=CTHRC1 PE=1 SV=1	26.2		1000			6 563 967
P02760	Protein AMBP OS=Homo sapiens OX=9606 GN=AMBP PE=1 SV=1	39	0.122	15.73	149 814	18 263	2 842 627
Q14195	Dihydropyrimidinase-related protein 3 OS=Homo sapiens OX=9606 GN=DPYSL3 PE=1 SV=1	61.9	1000	1000		89 536	542 310
P07858	Cathepsin B OS=Homo sapiens OX=9606 GN=CTSB PE=1 SV=3	37.8	0.001	10.65	61 154		1 562 756
A0A0U1RQV3	EGF-containing fibulin-like extracellular matrix protein 1 (Fragment) OS=Homo sapiens OX=9606 GN=EFEMP1 PE=1 SV=1	31.7	0.001	2.283	331 532		1 133 040

Downloaded from http://ahajournals.org by on October 1, 2021

Q9C075	Keratin. type I cytoskeletal 23 OS=Homo sapiens OX=9606 GN=KRT23 PE=1 SV=2	48.1	1000	1000		301 058	223 730
P60842	Eukaryotic initiation factor 4A-I OS=Homo sapiens OX=9606 GN=EIF4A1 PE=1 SV=1	46.1	7.99	3.315	23 958	327 983	215 830
Q8IZP2	Putative protein FAM10A4 OS=Homo sapiens OX=9606 GN=ST13P4 PE=5 SV=1	27.4		1000			423 965
Q9Y6C2	EMILIN-1 OS=Homo sapiens OX=9606 GN=EMILIN1 PE=1 SV=3	106.6					
H0YD13	CD44 antigen OS=Homo sapiens OX=9606 GN=CD44 PE=1 SV=2	22.7		1000			290 750
D6R9Z1	Receptor of-activated protein C kinase 1 (Fragment) OS=Homo sapiens OX=9606 GN=RACK1 PE=1 SV=8	26.3	1000	1000		190 818	441 593
Q6A163	Keratin. type I cytoskeletal 39 OS=Homo sapiens OX=9606 GN=KRT39 PE=1 SV=2	55.6	0.001	0.001	941 702		
P07360	Complement component C8 gamma chain OS=Homo sapiens OX=9606 GN=C8G PE=1 SV=3	22.3		1000			1 430 389
P04899	Guanine nucleotide-binding protein G(i) subunit alpha-2 OS=Homo sapiens OX=9606 GN=GNAI2 PE=1 SV=3	40.4		1000			867 424
Q9Y6R7	IgGFc-binding protein OS=Homo sapiens OX=9606 GN=FCGBP PE=1 SV=3	571.6		1000			605 189
P13639	Elongation factor 2 OS=Homo sapiens OX=9606 GN=EEF2 PE=1 SV=4	95.3	1000	1000		645 254	443 046
P29279	Connective tissue growth factor OS=Homo sapiens OX=9606 GN=CTGF PE=1 SV=2	38.1		1000			102 939
P13489	Ribonuclease inhibitor OS=Homo sapiens OX=9606 GN=RNH1 PE=1 SV=2	49.9	1000	1000		45 571	172 496
Q15404	Ras suppressor protein 1 OS=Homo sapiens OX=9606 GN=RSU1 PE=1 SV=3	31.5		1000			412 358
O94905	Erlin-2 OS=Homo sapiens OX=9606 GN=ERLIN2 PE=1 SV=1	37.8		1000			783 840
O14773	Tripeptidyl-peptidase 1 OS=Homo sapiens OX=9606 GN=TPP1 PE=1 SV=2	61.2		1000			873 519

Downloaded from http://ahajournals.org by on October 1, 2021

P55290	Cadherin-13 OS=Homo sapiens OX=9606 GN=CDH13 PE=1 SV=1	78.2		1000			2 967 442
P49908	Selenoprotein P OS=Homo sapiens OX=9606 GN=SELENOP PE=1 SV=3	43.2		1000			1 089 297
P27169	Serum paraoxonase/arylesterase 1 OS=Homo sapiens OX=9606 GN=PON1 PE=1 SV=3	39.7		1000			1 639 039
P55058	Phospholipid transfer protein OS=Homo sapiens OX=9606 GN=PLTP PE=1 SV=1	54.7		1000			642 557
P61158	Actin-related protein 3 OS=Homo sapiens OX=9606 GN=ACTR3 PE=1 SV=3	47.3	1000	1000		29 954	326 498
E9PDU6	Calponin (Fragment) OS=Homo sapiens OX=9606 GN=CNN3 PE=1 SV=1	20.2		1000			152 572
P05154	Plasma serine protease inhibitor OS=Homo sapiens OX=9606 GN=SERPINA5 PE=1 SV=3	45.6		1000			561 747
P33176	Kinesin-1 heavy chain OS=Homo sapiens OX=9606 GN=KIF5B PE=1 SV=1	109.6		1000			491 424
Q07065	Cytoskeleton-associated protein 4 OS=Homo sapiens OX=9606 GN=CKAP4 PE=1 SV=2	66		1000			481 910
P38646	Stress-70 protein mitochondrial OS=Homo sapiens OX=9606 GN=HSPA9 PE=1 SV=2	73.6	1000	1000		20 792	358 514
O00159	Unconventional myosin-Ic OS=Homo sapiens OX=9606 GN=MYO1C PE=1 SV=4	121.6		1000			134 782
B4DPQ0	Complement C1r subcomponent OS=Homo sapiens OX=9606 GN=C1R PE=1 SV=1	81.8		1000			60 192
P35555	Fibrillin-1 OS=Homo sapiens OX=9606 GN=FBN1 PE=1 SV=4	312.1		1000			406 352
Q9Y277	Voltage-dependent anion-selective channel protein 3 OS=Homo sapiens OX=9606 GN=VDAC3 PE=1 SV=1	30.6	1.034	4.162	26 367	27 256	811 053
Q96PD5	N-acetylmuramoyl-L-alanine amidase OS=Homo sapiens OX=9606 GN=PGLYRP2 PE=1 SV=1	62.2		1000			363 275
Q15084	Protein disulfide-isomerase A6 OS=Homo sapiens OX=9606 GN=PDIA6 PE=1 SV=1	48.1	1000	1000		15 615	198 018

Downloaded from http://ahajournals.org by on October 1, 2021

A0A0A0MS15	Immunoglobulin heavy variable 3-49 OS=Homo sapiens OX=9606 GN=IGHV3-49 PE=3 SV=1	13		1000			1 744 048
P24539	ATP synthase F(0) complex subunit B1 mitochondrial OS=Homo sapiens OX=9606 GN=ATP5PB PE=1 SV=2	28.9		1000			431 898
O75083	WD repeat-containing protein 1 OS=Homo sapiens OX=9606 GN=WDR1 PE=1 SV=4	66.2		1000			374 808
Q9UBC9	Small proline-rich protein 3 OS=Homo sapiens OX=9606 GN=SPRR3 PE=1 SV=2	18.1	1.549	0.001	179 655	257 193	
P15144	Aminopeptidase N OS=Homo sapiens OX=9606 GN=ANPEP PE=1 SV=4	109.5		1000			279 343
Q15019	Septin-2 OS=Homo sapiens OX=9606 GN=SEPT2 PE=1 SV=1	41.5		1000			377 432
P20073	Annexin A7 OS=Homo sapiens OX=9606 GN=ANXA7 PE=1 SV=3	52.7		1000			228 191
Q8N436	Inactive carboxypeptidase-like protein X2 OS=Homo sapiens OX=9606 GN=CPXM2 PE=2 SV=3	85.8					
Q5JR08	Rho-related GTP-binding protein RhoC (Fragment) OS=Homo sapiens OX=9606 GN=RHOC PE=1 SV=8	21.5		1000			905 779
Q99536	Synaptic vesicle membrane protein VAT-1 homolog OS=Homo sapiens OX=9606 GN=VAT1 PE=1 SV=2	41.9					
Q9NZN4	EH domain-containing protein 2 OS=Homo sapiens OX=9606 GN=EHD2 PE=1 SV=2	61.1		1000			1 898 281
B4DT28	Heterogeneous nuclear ribonucleoprotein R. isoform CRA_a OS=Homo sapiens OX=9606 GN=HNRNPR PE=1 SV=1	55.7		1000			651 320
B5MDF5	GTP-binding nuclear protein Ran OS=Homo sapiens OX=9606 GN=RAN PE=1 SV=1	26.2	1000	1000		102 675	1 558 912
Q8TF66	Leucine-rich repeat-containing protein 15 OS=Homo sapiens OX=9606 GN=LRRC15 PE=2 SV=2	64.3		0.001	214 171	674 082	

Downloaded from http://ahajournals.org by on October 1, 2021

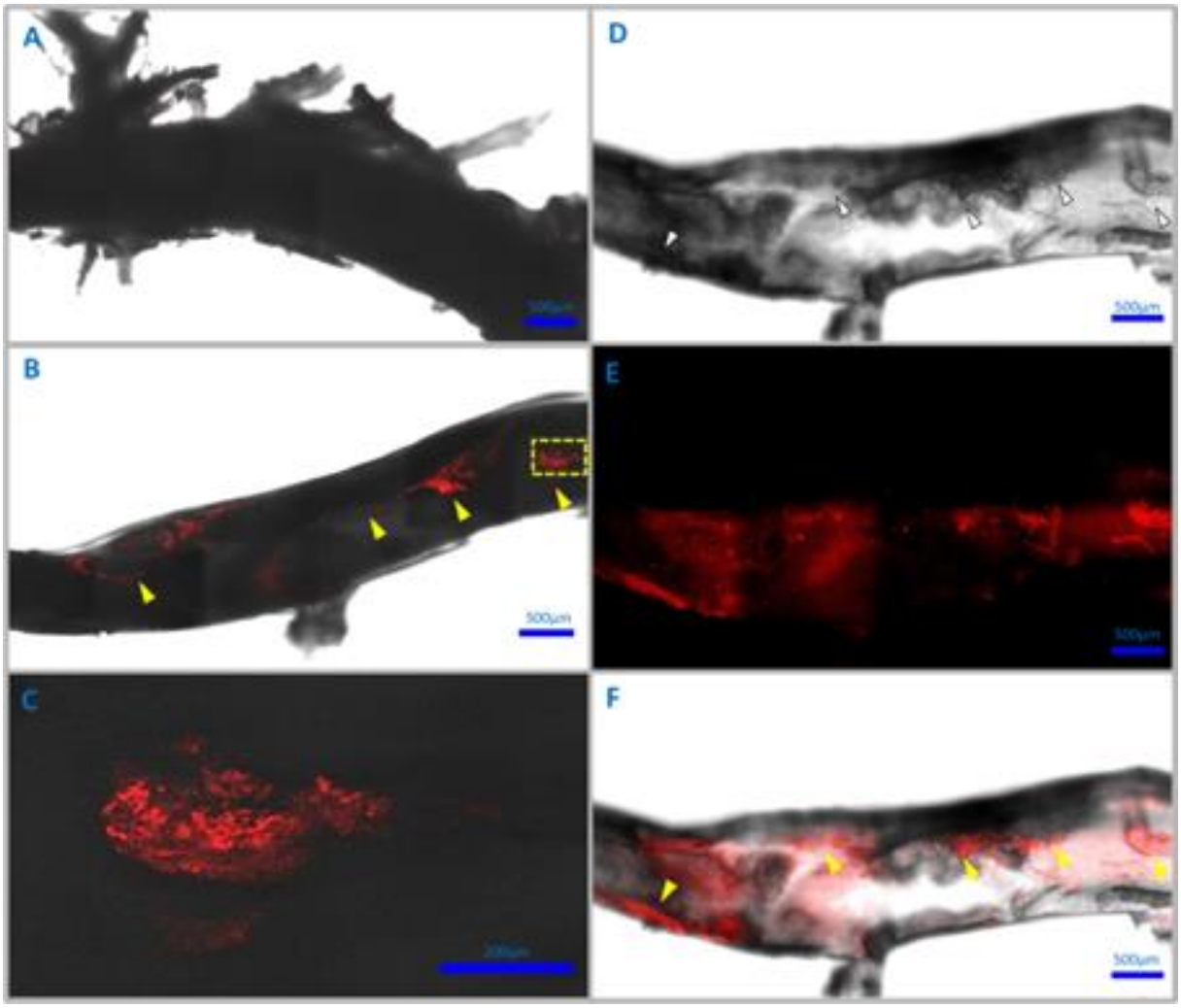
A0A0U1RRM8	Fermitin family homolog 2 (Fragment) OS=Homo sapiens OX=9606 GN=FERMT2 PE=1 SV=1	61.9		1000			1 449 577
Q92765	Secreted frizzled-related protein 3 OS=Homo sapiens OX=9606 GN=FRZB PE=1 SV=2	36.2		1000			7 510 093
Q08722	Leukocyte surface antigen CD47 OS=Homo sapiens OX=9606 GN=CD47 PE=1 SV=1	35.2		1000			2 008 365
P07093	Glia-derived nexin OS=Homo sapiens OX=9606 GN=SERPINE2 PE=1 SV=1	44		1000			582 320
J3QRN6	Unconventional myosin-Id OS=Homo sapiens OX=9606 GN=MYO1D PE=1 SV=1	111.2		1000			151 508
P02763	Alpha-1-acid glycoprotein 1 OS=Homo sapiens OX=9606 GN=ORM1 PE=1 SV=1	23.5	1000	1000		263 871	58 616
Q8IWU6	Extracellular sulfatase Sulf-1 OS=Homo sapiens OX=9606 GN=SULF1 PE=1 SV=1	101		1000			398 478
Q15746	Myosin light chain kinase. smooth muscle OS=Homo sapiens OX=9606 GN=MYLK PE=1 SV=4	210.6		1000			719 644
P84243	Histone H3.3 OS=Homo sapiens OX=9606 GN=H3F3A PE=1 SV=2	15.3	5.924	0.74	872 765	5 212 878	724 408
Q86VP6	Cullin-associated NEDD8-dissociated protein 1 OS=Homo sapiens OX=9606 GN=CAND1 PE=1 SV=2	136.3	2.101		4 458 635	9 368 130	28 020

Galectin-3 protein is highlighted in yellow

MW **[kDa]:** Molecular Weight in kDa**, Gal3Ab-Gal3R:** immunoprecipitate of anti-galectin-3 antibody with recombinant human galectin-3**, C4-PH:** immunoprecipitate of C4 scFv-Fc antibody with human endarterectomy proteins, **P3-PH:** immunoprecipitate of P3 scFv-Fc antibody with human endarterectomy protein

Downloaded from http://ahajournals.org by on October 1, 2021

Figure S1. *Ex vivo* imaging of P3 scFv-Fc in Apoe-/- (B, C, D, E, F) and wild-type (WT) mice (A) using confocal microscopes.



Confocal microscopy analysis was performed using P3 scFv-Fc coupled to Alexa-Fluor 648 dye after *ex vivo* injection in Apoe$^{-/-}$ and WT mice. A human IgG coupled to Alexa-Fluor 648 was used as negative control antibody. The presence of atheromatous plaques in the lumen of the aorta was observed in the Apoe$^{-/-}$ mouse (yellow arrowheads) (B, F). The yellow doted square corresponds to the enlarged view of P3 binding (C). The merged image was performed to show the localization of the fluorescence signal through the thickness of the aorta (F). Size bars (A, B, D, E, F): 500 µm; Size bars (C): 200 µm.

Downloaded from http://ahajournals.org by on October 1, 2021